Title

Cellular Mechanisms of Action Associated with Transcranial Ultrasound for Modulation and its Acoustic Characterization through Skull

Author

Babakhanian, Meghedi

Publication Date

2015

Peer reviewed|Thesis/dissertation

UNIVERSITY OF CALIFORNIA

Los Angeles

Cellular Mechanisms of Action Associated with Transcranial Ultrasound for Modulation and its Acoustic Characterization through Skull

A dissertation submitted in partial satisfaction of

the requirements for the degree Doctor of Philosophy

in Biomedical Engineering

by

Meghedi Babakhanian

2015

ABSTRACT OF THE DISSERTATION

Cellular Mechanisms of Action Associated with Transcranial Ultrasound for modulation and its Acoustic Characterization through Skull

by

Meghedi Babakhanian

Doctor of Philosophy in Biomedical Engineering

University of California, Los Angeles, 2015

Professor Warren Grundfest, Chair

Recent *in vivo* modulation of region-specific brain activity suggests that Low Intensity Focused Ultrasound (LIFU) may be a non-invasive alternative therapy for drug-delivery applications and the treatment of neurological diseases, including epilepsy and Parkinson's disease.

Despite these recent successes, failure to reproduce published results continues to plague the field due to the limited understanding of cellular mechanisms that underlie neuromodulation and the impact of skull on targeting accuracy. The objective of this thesis is to help bridge these knowledge gaps and better understand non-invasive transcranial focused ultrasound modulation.

While hypotheses exist explaining the mechanism underlying ultrasound modulation, they largely remain untested. It has been suggested that mechanical perturbation of cellular

membranes with embedded protein channels using ultrasound has an impact on ion channel kinetics, resulting in depolarization, and ultimately, increased neural activity. In particular, this thesis investigates the hypothesis explaining the mechanical perturbation as a result of pure acoustic radiation forces using simplified *in vitro* models, including Large-Conductance Mechanosensitive Channels (MscL) and non-mechanically stimulated channels. The outcome revealed an increase in efflux through proteoliposomes regardless of the channel type except at the highest concentration of mechanosensitive channel (MS) model where a lowering efflux trend was noticed. These unexpected results suggest that focused ultrasound does not modulate the gating of ion channels, but instead effects the permeability of the membrane itself or protein-membrane interface. Also a dual effect of membrane stretch enhancement and pore formation is observed only at high MS channel concentration.

In addition, to prepare for *in vivo* efficacy studies, the present dissertation characterizes the ultrasonic beam scatter and focal shifts that occur as ultrasound passes through a rat skull for a specific set of parameters. The results have shown significant beam shape deformation and target shift due to the skull.

This suite of studies improved our understanding of the mechanism associated with LIFU-based stimulation at the molecular level, while also exploring how LIFU can be applied with greater accuracy and precision *in vivo*. In addition, insights gleaned from this approach are expected to promote new avenues of clinical applications for the treatment of drug delivery, gene therapy and neurological illnesses.

The dissertation of Meghedi Babakhanian is approved.

Paul Blount

Wentai Liu

Nader Pouratian

Warren Grundfest, Committee Chair

University of California, Los Angeles

2015

This thesis is dedicated to my mom, dad, sisters, nephews and brother in-law , who have been my role models, given me endless encouragement and love, and have provided me with the motivation and skills to achieve the very best in life

Table of Contents

List of Figures

List of Tables

List of Equations

List of Acronyms

BBB – Blood Brain Barrier

BLS – Bilayer sonophore

CNS – Central Nervous System

CW – Continuous Wave

DBS – Deep Brain Stimulation

DC – Duty cycle

DF – Duty Factor

E – coli Escherichia coli

f – Frequency

FDA – Food and Drug Administration

FUS – Focused Ultrasound Surgery

FWHM – Full-Width at Half Maximum

HIFU – High Intensity Focused Ultrasound

I_{SPPA} – Intensity, Spatial Peak, Pulse-Average

I_{SPTA} – Intensity, Spatial Peak, Time-Average

LIFU – Low Intensity Focused Ultrasound

LPC – Lysophosphatidylcholine

MI – Mechanical index

MS – Mechanosensitive channel

MscL – Mechanosensitive channel of large conductance

MscS – Mechanosensitive channel of small conductance

NOC – Number of Cycles per Pulse

PD – Pulse Duration

PII – Pulse Intensity Integral

Pr – Peak Rarefaction Pressure

PRF – Pulse Repetition Frequency

PRF – Pulse Repetition Period

PRP – Pulse Repetition Period

PW – Pulse wave

TcMRgFUS – Transcranial MRI-Guided Focused Ultrasound Surgery

UCA – Ultrasound contrast agents

US – Ultrasound

VNS – Vagus Nerve Stimulation

LIST OF SYMBOLS

c – Velocity of sound [m/sec]

D – Wave displacement [m]

f – Sound wave frequency [Hz]

I – Time-averaged intensity [W/cm^2]

I_i – Instantaneous Intensity

K – Wave number [m^{-1}]

P – Acoustic pressure [Pa]

t – Time [sec]

T – Time period [sec]

z – Acoustic impedance [$kg/sec\ m^2$]

α – Absorption coefficient [m^{-1}]

λ – Wavelength [m]

ρ – Density [kg/m^3]

ω – Angular frequency [sec^{-1}]

ACKNOWLEDGMENTS

The following dissertation could not have been completed without the support, guidance, assistance, and mentorship of many advisors, colleagues, collaborators, friends, and family over the years.

I would like to express my deepest appreciation to my committee chair and PhD advisor, Dr. Warren Grundfest, whose support, knowledge, and vision have been integral to both the success of this project and my graduate education. His mentorship and ambitious attitude have helped me shape my future goals and interests.

Part of my thesis was conducted through a collaboration with Dr. Paul Blount's lab from University of Texas, Southwestern Medical School in Dallas. I wish to express my sincerest thanks to Dr. Blount for an amazing collaborative experience. He was open to trying out new methods and provided me with all the necessary facilities while I was visiting for our joint research work.

A very special thanks goes out to Dr. Bryan Nowroozi, without whose guidance, motivation and encouragement my project results would have been impossible. It was under his tutelage that my thesis was shaped, obstacles were addressed methodically and milestones were achieved.

I am deeply indebted to Dr. Limin Yang, from Dr. Paul Blount's lab, for her critical role in conducting the *in vitro* experiments, preparing vesicles and proteins, and proteoliposomes. She also consulted with me on the analysis of the data and reporting results. She contributed large amounts of her time, and the success of the *in vitro* results would have been impossible without her efforts.

Besides my advisors, I would like to thank my committee members, Dr. Wentai Liu and Dr. Nader Pouratian, for their expert opinion, insightful comments, questions and support.

I would also like to acknowledge Dr. George Saddik for his contribution to the system electronics and transducer matches as well as guidance and support, and Dr. Martin Culjiat and Rahul Singh's support during the initial years of my project.

In addition, a special thank you to Dr. Ligia Toro, Dr. Enrico Stefani, Dr. Riccardo Olcese, Nicolleta Savalli, Shahab Danesh, Harpreet Singh, and Min Li for offering me their labs, teaching me wet lab techniques, transfection, cell preparation, and patch clamp work and, finally, being supportive of my project.

I am also grateful to my graduate student coworkers and friends, without whom my graduate experience would have been empty and impossible to survive: Richard, Pria, Zach, Jun, Alan, Dave, Justin, Dr. Dutson, Nathan, William, Marko, Ani, Nare, Talar, Lena, Palig, Arda, Noushig, Nareeneh, and Ooshatsank.

There are three members from my lab who I would like to especially thank for their unlimited amount of support throughout my graduate years. Neha Bajwa, who is an extraordinary and smart friend/coworker and has always been supportive of me in both personal and professional matters. She has shown me the true meaning of high quality work. Jim Garritano, who provided me with extensive programming and statistical analysis skills and kept me sane during my many sleepless nights. Last, but not least, Ashkan Maccabi, who helped me with matching networks for my system and provided endless support.

I would like to thank Dr. Alexander Bystritsky, who introduced me to the transcranial ultrasound neuromodulation field. My sincerest thanks also go to Dr. William Melega, one of my

advisors on the biophysics and neuroscience aspects of this project. He introduced me to the *in vitro* and *in vivo* aspect of this work and trained me in conducting true scientific research.

The undergraduates and other team members, who contributed to the experimental preparation, testing, data analysis, and support, have been invaluable in the completion of my studies, including Dina Drabidian, Lillian Boodaghians, Sayonika Mohanta, Sam Marton. and Kaitlyn Irelan.

Finally, I would like to thank my family and friends for their endless support and encouragement despite the obstacles we faced during my graduate years. I was able to pursue my passion because of their selfless attitude, and I would not have been able to get this far without their guidance and support in life.

I recognize that this research would not have been possible without the financial assistance of Journal of Cell Sciences (JCS) Travel grant, UCLA travel fellowship, Jean Perkins Foundation, and Cancer Prevention & Research Institute of Texas (CPRIT Grant) through Dr. Blount's efforts.

VITA

EDUCATION

University of California Los Angeles, CA • Master of Science, Bioengineering 2011
Sep 2009-Sept 2011
Affiliations: Graduate Researcher, UCLA Center for Advanced Surgical and Interventional Technology (2010-2015)

University of California, San Diego, CA • Bachelor of Science, Mechanical Engineering
Sep 2004 – Sep 2006

CONSULTING EXPERIENCE

UCLA Harbor Medical Center *Los Angeles, CA*
Medical Device Technical Advisor and Consultant *Aug 2014 –Present*

INDUSTRY EXPERIENCE

Boston Scientific Neuromodulation *Valencia, CA*
Manufacturing Engineer II *March 2009-Aug 2009*

Second Sight Medical Products *Sylmar, CA*
R&D and Manufacturing Engineer *Sep 2007 –Jan 2009*

ENTREPRENEURSHIP EXPERIENCE

UCLA Office of Intellectual Property & Industry Sponsored Research *Los Angeles, CA*
Technology Transfer Fellow *Sep 2012 –March 2013*

UCLA Business of Sciences Center (BOS) - Venture Capital Funding Competition *LA, CA*
Technology Investment Investigator and Presenter *March 2012 –June 2012*

TEACHING & MENTORSHIP EXPERIENCE

Glendale Community College, Dept. of Engineering *Los Angeles, CA*
Adjunct Professor *Feb 2014 –Present*

UCLA Dept. of Engineering and Bioengineering *Los Angeles, CA*
Teaching Fellow *Sep 2009 –July 2014*
Teaching fellow specializing in Design of Minimally Invasive Medical Technology course and translation of devices from bench to clinic, Physiology, Bioengineering laboratory skills, Introduction to Bioengineering, and Engineering Writing.

National Science Foundation (NSF) K-12 Education Outreach- Culver City High School
Culver City, CA
Graduate Teaching Guest Instructor *June 2012 –June 2013*

SELECTED PUBLICATIONS

- **Babakhanian, M.,** Yang, L., Nowroozi, B, Garritano, J., Saddik, G., Maccabi, A., Boodaghians, L., Blount, P., Grundfest, W "Cellular Mechanisms of Action Associated with Low Intensity Focused Ultrasound Neuromodulation" Society of Brain Mapping and Therapeutics (SBMT) 12th Annual World Congress Abstract, Los Angeles, CA., Focused ultrasound session, March 6-8, 2015

- **Babakhanian, M.**, Nowroozi, B, Garritano, J., Saddik, G., Maccabi, A, Grundfest, W, "Acoustic Characterization of Low Intensity Focused Ultrasound System through Skull" 4th International Focused Ultrasound Symposium, Bethesda, MD. 12-16 Oct 2014.

- Mulgaonkar, A., **Babakhanian, M**., Culjat, M., Nowroozi, B., Melega, W., Grundfest, W., "Characterization of Transcranial Ultrasonic Passage in the Göttingen Minipig" Proceedings of 2014 IEEE Ultrasonics Symposium, Chicago, IL. 3-6 Sep 2014.

- **Babakhanian, M**, Nowroozi, B, Saddik, G., Maccabi, A, Grundfest, W, "Low Intensity Focused Ultrasound Acoustic Characterization through Skull" 7th Image Guided Therapy Workshop, MIT, Cambridge, MA. 18 September 2014.

- **Babakhanian, M.**, Fan, R., Mulgaonkar, A., Singh, S., Culjat, M., Danesh, S., Toro, L., Grundfest, W., Melega, W. (2012) "In-vitro cell system for studying molecular mechanisms of action associated with low intensity focused ultrasound", proceedings of SPIE Photonics West-BIOS: Advanced Biomedical and Clinical Diagnostic Systems X, Medical Devices and Methods Session, San Francisco, CA, 23 Jan 2012.

- **Babakhanian, M**. et al.. "Acoustic Characterization of Low Intensity Focused Ultrasound System through Rat Skull" 14th Annual UC System-wide Bioengineering Symposium., University of California, San Diego, CA. 20 June 2013.

- Book Chapter : Culjat M. O., Fan R. E., **Babakhanian M.**, Mulgaonkar A. P., Singh R. S., Grundfest W. S., Melega W. P.. "Focused Ultrasound for Non-invasive Neuromodulation" Nanoneuroscience and Nanoneurosurgery, Ed. Kateb B. and Heiss J.. Maryland: Taylor & Francis Group, 2013. Chapter 15. Print.

AWARDS & SCHOLARSHIPS & FELLOWSHIPS & GRANTS

- Certificate in the Business of Science, University of California, Los Angeles April 2015
- Ursula Mandel Bioengineering Scholarship Sep 2014-June 2015
- Mangasa M. Mangasarian UCLA Graduate Student Scholarship Sep 2014-June 2015
- Armenian General Benevolent Union Scholarship Sep 2014-June 2015
- UCLA Pilot Travel Fellowship Sep 2014-Dec 2014
- Journal of Cell Science Travel Grant June 2013-June 2013
- National Science Foundation (NSF), Graduate Teaching Fellows in K-12 Education June 2012-June 2013
- University of California, Los Angeles, The Affiliates of UCLA Scholarship June 14,2011
- Armenian Professional Society Scholarship Dec 10,2010
- ARS Samuel and Aghavni Eremian Scholarship for community involvement Sep 01,2009

1 Introduction

1.1 Current Neuromodulation Therapies

Therapies for neurological or psychiatric diseases are presently limited to pharmacologic or invasive surgical strategies. Each of these approaches has inherent limitations. For example, drugs that have been designed to target a particular neurotransmitter system function or parameter still lack regional selectivity (e.g., SSRIs affect all serotoninergic synapses in the brain). Further, there can be adverse effects associated with drug use (e.g., SSRIs – nausea, sexual dysfunction, weight gain) as well as concerns about drug metabolism and clearance in individuals with compromised hepatic and renal. Conversely, neurosurgical interventions such as deep brain stimulation (DBS) and resection can target specific brain regions but are invasive and have an associated morbidity risk [1]. Many novel non-invasive therapies such as repetitive transcranial magnetic stimulation (rTMS) [2-4], transcranial direct current stimulation (tDCS) [5], and Trigeminal Nerve Stimulation (TNS) [6], and are being explored as treatments for Epilepsy, but are still in the research phase [4, 7].

For these limitations, there has been an increased attention on possible use of focused ultrasound as a means for noninvasive neuromodulation therapy. Early indications of ultrasound effects on excitable tissue date back many decades. Recently, Low Intensity Focused Ultrasound (LIFU) has shown potential similar effects to the current neuromodulation methods, though with somewhat variable success rates. Given this limited success rate, LIFU could dramatically increase the range of treatments. We hypothesize that the variability in results and limited success rates that have been reported may be a result of the lack of knowledge regarding the mechanism underlying modulation, effective parameters and the accuracy and precision of

targeting. Our research objective is to demonstrate the mechanism explaining ultrasound modulation at the cellular level and to characterize beam deformation and deflection due to skull to improve precision and accuracy, and ultimately efficacy for successful preclinical and clinical ultrasound neuromodulation.

1.1.1 Low Intensity Focused Ultrasound (LIFU)

In recent years, Low Intensity Focused Ultrasound (LIFU) has made great strides in the realm of non-invasive neuromodulation [8-10]. LIFU has been shown to effectively stimulate both neurons in culture and a short-latency excitatory response in a rodent brain-slice assay [11, 12]. In addition, the use of LIFU *in vivo* has resulted in compelling evidence of neuromodulation of the motor cortex in the mouse, leading investigators to believe that LIFU may be a competing candidate to replicate the effect of current prominent treatments, and more invasive, mechanisms of neuromodulation for conditions such as Parkinson's disease and Epilepsy [8, 11]. Despite these recent successes, skull effect on targeting especially after transitioning to human brain and the underlying cellular mechanisms explaining LIFU neuromodulation remain unknown and limiting factors for successful repeatable results.

1.1.2 Cellular Mechanism Underlying LIFU Neuromodulation

It is thought that mechanical perturbation of neuronal cellular membranes, or proteins embedded in these membranes, has an impact on ion channel kinetics leading to depolarization, and ultimately, increased action potential discharge [9, 13]. Two hypotheses have been put forth suggesting that the development of this mechanical perturbation is either (1) a result of the formation and collapse of gaseous cavitation bubbles adjacent to cell membrane causing membrane modulation or (2) a result of the acoustic radiation force associated with the

propagation of acoustic waves through an attenuating medium translated into the cell membrane [9, 13, 14].Prior studies indicate that many voltage-gated ion channels show mechanosensitive properties that render their gating kinetics sensitive to transient changes in lipid bilayer tension [12]. Also exposing fibroblasts in culture to ultrasound induced a reversible increase in intracellular Ca^{2+} concentration supporting the hypothesis that ultrasound is modulating ion channel gating [13]. These studies were conducted using parameters that didn't induce cavitation and also no manual injection of microbubble/cavitation was performed in the latter investigations. Therefore, the present thesis hopes to clearly test the non-cavitational hypotheses to determine the underlying cellular mechanism of focused ultrasound modulation as well as the most effective FUS parameters causing these biological effects.

These results will be subsequently translated into a limited number of parameter sets for future *in-vivo* studies in which the effects of LIFU on neuronal inhibition and excitation firing patterns in animal models of neurological disorders will be assessed.

2 Ultrasound Applications and Background

2.1 Motivation

The neuromodulation market is expected to be as high as $6.8 Billion by 2017. This market growth is due to higher incidences of endemic diseases, rise in aging population and related diseases (Alzheimer's, epilepsy, spinal cord injury, and Parkinson's disease), promising clinical trials for new technological advancement and demand for a better and less invasive neuronal control modality. According to the International Neuromodulation Society, about 40 million to 50 million patients worldwide suffer from epilepsy. As of 2012 about 1.5 million people suffered from Parkinson disease in the U.S. The large pool of patients that suffer from depression, stroke, anxiety disorders, lower back pain, urinary incontinence, and tremor offers the neuromodulation industry opportunities to grow in the next five years (Market Studies 2013). Despite the rising demands, there are significant limitations associated with the current therapeutic approaches to CNS disorders. Nevertheless, each one of the existing therapies for human neuromodulation have substantial drawbacks as mentioned in the previous chapter. Thus, there is a great need for innovative strategies that can treat and reduce CNS disorders such as seizure activity and induce neuromodulation as alternatives to drug-based, surgical interventions and non-invasive modalities. As a result of this demand, LIFU was considered as a possible neuromodulation technique.

Ultrasound has long been part of the modern medicine practice. Ultrasound waves are pressure waves that propagate through a medium with a frequency greater than 20 kHz. Although the imaging and monitoring application of ultrasound is well known, there are other applications of ultrasound such as therapeutic. Therapeutic ultrasound is categories by Low or High Intensity ultrasounds. These categories cause thermal or non-thermal effects although

sometimes the effect isn't easily differentiable. The frequency varies from 0.7-3MHz in therapeutic ultrasound and with maximum energy absorption occurring at depths between 2 and 5 cm [15].

2.2 Noninvasive Therapeutic Ultrasound

2.2.1 HIFU and Applications

High-intensity focused ultrasound (HIFU) has been suggested for use as a tool to target and ablate subcutaneous tissue volumes by localized heating, specifically as a potential therapy tool for soft tissue tumors [16, 17]. Focusing allows ultrasound to travel harmlessly through tissues outside the focal zone of the transducer due to the low energy density in these regions, while heating and sometimes ablating tissues such as tumors within the focal zone. The focused acoustic waves heat up the tissue to temperatures as high as 70°C for 1–3 s at intensities in the 1 kW/cm^2 range [18]. This temperature threshold is identified to cause coagulative necrosis and immediate cell death [19-21].

HIFU is now approved by the Food and Drug Administration (FDA) for heating and ablating uterine fibroids in the United States. In other countries, it is used to treat prostate and bone cancers [22].

2.2.1.1 Focused Ultrasound Ablation Background (HIFU)

The use of ultrasound has been previously proposed to reversibly modulate function in the CNS [23-26] and also explored the possibility of inhibiting peripheral nerve conduction [23, 27]. For example, a successfully induced permanent nerve block on a rabbit sciatic nerve was shown *in-vivo* using high intensity (>1.5 kW/cm^2) and 30s-long, continuous sonication [28]. As discussed in previous chapters, the mechanism associated with HIFU systems is most commonly attributed to thermal effects [21].

The primary impediment to using ultrasound in the brain, whether for therapeutic or imaging purposes, has been the cranium. Early attempts at producing lesions in the brain through the intact skull bone were unsuccessful [29, 30]. Propagation through the cranium results in significant distortion and attenuation of the acoustic beam, thereby limiting accuracy of the procedures and also increasing potential health risks to the patient. Due to complications of FUS transmission through the skull, many earlier ultrasound research efforts were therefore performed invasively through a window in the skull following craniotomy. Patients with Parkinson's disease were among the first to be treated with HIFU performed through a craniotomy [23, 31]. Although the treatment helped ameliorate some Parkinson's symptoms, this research was not further pursued because of the requirement to remove a section of the skull and difficulties in obtaining accurate targeting.

It wasn't until 2010, that a neurosurgical noninvasive HIFU systems, the ExAblate, became commercially available via Insightec (Haifa, Israel). This system combines visualization of soft tissues, temperature sensitivity, and guidance of MRI with using phased array focused transducers to provide compensation for ultrasonic distortion through the skull [32]. Recent research has demonstrated the clinical feasibility of transcranial MRI-guided focused ultrasound surgery (TcMRgFUS) using the ExAblate system. The feasibility of transcranial targeting with noninvasive FUS ablation was also demonstrated, although clinical outcomes were mixed due to insufficient power [17]. Despite these issues, in more recent studies, ultrasonic treatment showed promising thalamotomy results through an intact human skull [33, 34]. Much work is still required, to further advance high-power systems for effective ablation at different tissue depths and also in defining safety margins to deliver energy selectively without overheating the skull.

Within the past 50 years, the FUS therapeutic studies expanded to different neural structures conducted at varying acoustic intensities and stimulation durations. Ballantine and Bell *et al*. explored the potential of ultrasound for nerve conduction inhibitory effects and pain management purposes [35]. Soon after, Young and Henneman demonstrated these effects on cat saphenous nerve bundles[36]. These studies were followed by focused ultrasound stimulation and nerve modulation studies in mammals and human subjects by Russian researchers [25, 37-40]. In addition to older studies, Mihran and colleagues (1990) reported neuronal modulation in peripheral nerves of a frog using relatively short irradiation by delivering peak intensities ranging from 100-800 W/cm^2 (delivering 500 μs ultrasound (US) pulses of 2.0–7.0 MHz) [41] .

However, because excessive heat and pressure associated with HIFU may damage brain tissue, low-energy pulsed application of focused ultrasound sonication (i.e., LIFU) was alternatively suggested for the reversible neuromodulation application. The modality of LIFU has only recently been advanced for consideration of clinical applications with the advent of superior ultrasound instrumentation and brain MR imaging that would allow for accurate and safe targeting in humans.

2.2.2 LIFU and Applications

Low Intensity ultrasound is used for physical therapy of conditions such as osteoarthritis, carpal tunnel syndrome, and tennis elbow. In these cases the ultrasound is applied for 10 min at intensities in the 1W/cm^2 range which won't raise the tissue temperature above ~38ºC [18]. Staying around the same range of intensities, around 50 mW/cm^2, fracture healing enhancement is another application of Low Intensity ultrasound [42].

2.2.2.1 LIFU Background

Lower-energy application of focused ultrasound sonication showed bullfrog sciatic nerve stimulation at temporal average intensity of 1 W/cm^2 continuous wave (5 min US at 3.5 MHz) while 2 and 3 W/cm^2 decreased the action potential amplitudes [43].

To induce bioeffects without producing thermal effects and tissue damage, many studies have proposed acoustic intensities <500 mW/cm^2 [21, 44, 45]. Tyler demonstrated neurostimulation in hippocampal slice cultures and *ex vivo* mouse brains using low intensity Low Frequency Ultrasound (LILFU) [12]. Later, Tufail and his colleagues performed *in vivo* studies on an intact mouse brain targeting the hippocampus using unfocused transducers which caused motor activity. They recorded Local field potentials (LFP) and multiunit activity (MUA) while stimulating the primary motor cortex using pulsed ultrasound at an intensity of 36.20 mW/cm^2 I_{SPTA} and a frequency of 350 kHz. At intensity of 64.53 mW/cm^2 I_{SPTA} and a frequency of 500 kHz they noticed tail twitching and EMG activity in the lumbosacrocaudalis dorsalis lateralis muscle. lower I_{SPTA}= 42.90 mW/cm^2 and frequency of 350 kHz triggered an EMG response at the contralateral triceps brachii muscle. At I_{SPTA}=84.32 mW/cm^2 and frequency= 250 kHz significant increase in spike frequency was noticed. With these studies, Tyler was able to conclude that lower frequencies were found to produce more robust EMG responses, and no measureable BBB disruption was observed during the course of the study with I_{SPTA} up to 142.20 mW/cm^2 [46].

Yoo and his colleagues explored FUS-mediated regional modulation of neural tissue excitability *in vivo*. The results were bimodal meaning the brain activity can be stimulated and selectively suppressed. Yoo monitored the modulation effect by both electrophysiological recordings and fMRI. The motor activity detected both by visual inspection and electrophysiological recording were using 690 kHz frequency and I_{SPTA} of 6.3 W/cm^2 (12.6

W/cm^2 I_{sppa}). The I_{SPTA} used for the blood-oxygenation-level-dependent (BOLD) activation was 1.6 W/cm^2 (I_{sppa}=3.3 W/cm2) which is much lower than the intensity that resulted in motor activity. However, the effective intensity levels found were higher than what Tyler and Tufail reported in their experiments and that could be due to anesthetic level, animal size, frequency and type of ultrasound chosen. Yoo also demonstrated visual activity suppression by administering shorter TBD and I_{SPTA}=160 mW/cm^2 (I_{sppa} of 3.3W/cm^2; 5% duty cycle). These results show that the time-averaged acoustic intensity (I_{SPTA}=160 mW/cm2) for suppression of activity was 10 times smaller than those used in excitatory sonication (I_{SPTA}= 1.6 W/cm2). Thus longer ultrasound exposure (by order of seconds or minutes) with shorter pulses (reducing duty cycle) causes less stimulation of neurons. Also, these neuronal stimulations were confirmed to cause no BBB disruption and purely due to the non-thermal mechanical effects of the local brain tissue [47].

Yoo and his colleagues continued their studies using low-intensity transcranial focused ultrasound (FUS) in 2012 by modulating the abducens nerve which caused the corresponding abductive ipsilateral eyeball movement in rats. The acoustic intensity causing stimulation in this study were as follows: frequencies=350 kHz, I_{SPTA}=4.6 W/cm2 [48]. This intensity was comparable to the intensity used in studies performed in 2011 that caused excitation of the motor area of the rabbit brain (6.3 W/cm^2 I_{SPTA}) [48], suggesting that acoustic intensity, on the order of 4.6–6.3 W/cm^2 I_{SPTA}, successfully stimulates both brain tissue as well as the cranial nerves with no BBB disruption as well as no damage to the nerves and adjacent brain tissue.

Finally, Yoo, Min and their colleagues were able to use Low Intensity, pulsed focused ultrasound (FUS) to non-invasively suppress an epileptic activity in a rat. These sonication were applied to the thalamic areas of the brain using a focused ultrasound operating at 690kHz and

I_{SPTA} of 130 mW/cm^2 (corresponded to 2.6W/cm^2 in terms of I_{sppa}).The results revealed that low-intensity, pulsed FUS sonication decreases the epileptic behavior, as assessed by the Racine score [10].

Recent data from King's lab studied higher intensity transcranial neurostimulation of the mouse somatomotor, using unfocused ultrasound. King explored continuous vs. pulsed stimulation and he studied sonication using I_{sppa} as high as 4.2,12.8, and 16.8 W/cm^2. He also studied a range of frequencies. He was able to obtain good EMG results at an I_{sppa} of 16.8 W/cm^2 applied for 80 ms. They concluded that continuous-wave stimuli are as effective as or more effective than pulsed stimuli and also stronger stimulus intensities and durations increase the probability of a motor response without affecting the duration or strength of the response [8]

2.2.2.2 Mechanisms Explaining the Biological Effect

The limited success in the *in vivo* studies of LIFU neuromodulation is due to the lack of the understanding 1- the cellular mechanism driving this LIFU-induced neuromodulation, 2- the effective parameters and 3- the knowledge of transcranial targeting. While our ultimate goal is to study and optimize LIFU applications in humans, systematic studies of underlying molecular mechanisms that drive this neuromodulation innovation as well as spatial distribution of the beam have yet to be conducted.

As mentioned before, heating the tissue via absorption of the focused acoustic waves is one of the common mechanisms in ultrasound applications. The other mechanism of this application is non-thermal which includes acoustic streaming, cavitation and mechanical oscillation. Acoustic streaming is the shear stress introduced onto the cell surface due to a localized flow of liquid around bubbles in contact with the cell. Cavitation is introduced by the

expansion, contraction and bursting of microbubbles in tissues that cause shockwaves that disrupt or damage cells.

Ultrasound works therapeutically through either thermal or mechanical effects on the target tissue. These effects and their biological outcomes depend on the type of tissue (muscle vs. bone) and the ultrasound parameters (Continuous or pulsed, power, duration and PRF). As mentioned earlier, in my studies we concentrate on the non-thermal effects.

The prevailing hypothesis explaining the non-thermal interaction of ultrasound energy and tissue is that the pressure transmitted to the tissue creates nanometer-scale deformation of the cell or the neuronal membrane. This pressure could cause modulation of ion-channels and mechanoreceptors embedded within the membrane leading into cellular excitability, potential variation, neurotransmitter release, uptake, and a general modification of neural circuits [9, 12, 49].

The pressure transition to the tissue is mediated by one or a combination of the following two mechanisms: 1) Cavitation phenomena: which is the interaction of ultrasound acoustic energy with microbubble creation within a medium, oscillation, growth and collapse of those microbubbles under appropriate acoustic parameters that induce modulation [8] and 2) non-cavitation phenomena: which involves the acoustic radiation force propagating through the tissue and inducing modulation [14].

2.2.2.3 Cavitation mechanism

The cavitation mediated ultrasound effects is due to acoustic energy interaction with microbubbles in the tissue. These microbubbles may be injected into the tissue or the blood stream or they can be generated in tissue due to the sharp change in local pressure caused by

ultrasonic transmission. Gas pockets formed in the tissue could either inertly scatter the acoustic waves propagating the medium or by oscillation.

Gas pockets cause scattering of the acoustic wave due to the impedance difference between the bubbles and liquid medium. In order for the gas pockets to scatter the acoustic wave, the US wavelength will need to be much less than the bubble's radius. Since the bubbles created due to ultrasound are much smaller they will act as oscillators rather than sources for scattering. Bubbles going through oscillation can either generate stable cavitation (non-inertial cavitation) or inertial cavitation.

Stable cavitation is the type when microbubbles grow and shrink with the pressure changes of ultrasound. Steady fluid flow (micro-streaming) is created around the bubbles due to the non-homogenous periodic field [50] . The flow strength and the distance from the bubble surface create the shear stress felt by the neighboring cell which could be deforming the cell. Under appropriate acoustic frequency, bubble size and high enough negative ultrasonic pressure, stable cavitation bubbles can collapse which is called inertial cavitation. Inertial cavitation can cause tissue damage.

King *et al*. reports *in vivo* transcranial stimulation of the nervous system with continuous wave ultrasonic radiation, I_{SPPA} more than 10 W/cm^2. They explain the mechanism underlying the neuronal modulation using the cavitation phenomena [8].

Also, bilayer membrane model designed by Krasovitski *et al*. support the cavitation formation and collapse hypothesis. The model predicts that the cellular membrane can transform mechanical energy from the ultrasound into expansions and contractions of the intramembrane space. These model predictions were experimentally supported by *in vivo* gold fish epidermis

studies which were exposed to CW ultrasound at 1MHz and 3 MHz, max I_{SPTA}=2.2 mW/cm^2 [49].

2.2.2.4 Non-cavitation mechanism (Acoustic radiation force)

Nevertheless, the cavitation hypothesis has major limitations since Tyler *et al*. was able to show biological effects induced by low intensity and low frequency ultrasound (I_{SPTA} of <100 mW/cm^2) with no signs of cavitation [12, 44, 45]. Tyler *et al*. showed stimulating neurons and network activity via mechanical deformation of neuronal cell membranes or proteins embedded in the membranes. The results from the *in vitro* hippocampus slices showed activation of voltage-gated sodium and calcium channels explaining the excitation of neurons [12].

We assume that the cavitation phenomenon isn't relevant in our investigations because of the chosen range of parameters. Our interest is with low frequency and low intensity acoustic values which interact with the biological tissue via non-thermal and non-cavitational mechanism.

A detailed parameter studies and better molecular mechanism understanding of the ultrasound interaction with a cell membrane (with or without embedded mechanosensitive channels) will help improve, discover and develop new applications of low intensity ultrasound. These applications include tissue and nerve modulation, BBB permeabilization, gene transfection and drug delivery through modulation.

In the hopes of explaining the mechanism underlying low intensity low frequency ultrasound (LILFU) modulation of neuronal activity, Tyler investigated the influence of US on neuronal activity at the cellular level by monitoring ionic conductance in individual neurons and synaptic transmission from release sites. He used a 440 kHz flat transducer that generated a pulse average intensity (I_{PA}) of 2.9 W/cm^2 and a temporal average intensity (I_{TA}) of 23 mW/cm^2. Tyler demonstrated that ultrasound sonication activated voltage-gated Na^+ and Ca^{2+} channels which

altered the membrane potential and initiated nerve conduction. He also showed that changes caused by LILFU in neuronal activity were enough to trigger SNARE-mediated synaptic vesicle exocytosis and synaptic transmission at central synapses leading to network activity [12].

Recent ultrasound efforts focused on stimulating cells and tissues using low-intensities in variety of applications (up to 3 W/cm^2). As mentioned earlier, Low intensity ultrasound has been used to accelerate fracture healing processes and for physical therapy purposes [42]. In addition, these lower intensities have shown enhancement in transdermal drug delivery [51]. Further studies of low intensity ultrasound at the cellular level demonstrated ultra-structural changes in tumor cells [52], cellular membrane property alterations, membrane permeability and cell proliferation through gene regulation [53-55].

Low intensity and low frequency ultrasound irradiations have been widely studied in the microbiological organisms. Bacterial biofilm usually colonize chronic transdermal and completely implanted medical devices such as catheters, electrical leads, drug delivery tubing, heart valves, prosthetic joints and other polymeric and metallic implants. It is common practice to control most of the cases mentioned above using antibiotic therapy but it's almost impossible to treat the entire infection. This is due to the biofilm environment protecting the bacteria from being killed by the antibiotic. Thus the infection reappears when the antibiotic therapy is stopped and the device needs to be removed to stop the infections. Low Intensity ultrasound studies have shown promising results in enhancing the antibiotic action on mostly gram-negative bacteria in vitro and in vivo. Gram-positive bacteria has shown more resistance to ultrasound and antibiotic treatments [56, 57].

2.3 Aim

We propose to built a simplified *in vitro* model and ultrasound systems where we could easily vary parameters and test LIFU non-cavitational modulation hypothesis on membrane and protein channel interaction. These studies as well as our transcranial ultrasound beam characterization studies for better non-invasive targeting will help with future *in vivo* studies in the field.

2.4 Innovation

Successful demonstration of controlled focused ultrasound modulation of CNS circuits can potentially be one of the non-invasive solution for the clinical treatment of various psychiatric and neurological disorders, including major depressive disorder, schizophrenia, sleep disorders, dementias, movement disorders, epilepsy, and neuropathic pain.

The results of this research will provide experimental evidence for ultrasound modulation molecular mechanism, thereby providing the scientific justification for future *in vivo* studies exploring the long term targeting, safety and efficacy of ultrasonic neuromodulation. Once the operating parameters are optimized for *in vitro* studies, these results can be used to assess the effects of neuronal inhibition and excitation on neuronal firing patterns associated with seizure activity and CNS disorders

3 Ultrasound System

3.1 Ultrasound

Ultrasound's diagnostic imaging modality has been clinically used since the 1960s. During this time, research in the bioeffects and therapeutic applications of ultrasound was also conducted. Initial ultrasonic bioeffect was noticed through a test against a frog model [14] and later through focusing the ultrasound energy in the brain with minimal effects to surrounding tissues [23].

One of the hypotheses explaining the nonthermal therapeutic effects of ultrasound at the molecular level is the cavitation (gas bubbles) formation that apply steady pulsation onto the cell or it could collapse rapidly that could damage cells [58]. However, low intensity nonthermal and non-cavitational ultrasound exposures have also shown bioeffects in cells and tissues.

To pursue my studies, my team and I at Center for Advanced Surgical and Interventional Technology (CASIT), UCLA, have been involved in the design and development of various ultrasound probes with varying parameters such as frequency, intensity, pulse duration and total energy delivered. We have developed ultrasound probes for both *in vivo* use, in rat and pig models, as well as *in vitro* probes, that are cell plate and patch clamp system compatible [59]. Unfortunately, there are no commercially available probes that are compatible with the patch clamp system and well plates, especially for small well diameter sizes for submerging purposes. The ones available are most commonly optimized for ultrasound cleaning, medical imaging and non-destructive testing (NDT).With regards to the present study, I have designed, fabricated, and characterized a functioning LIFU probe compatible with cell culturing plates and flasks. Also, my lab worked on a probe of the size necessary to accommodate patch clamp studies and invasive *in vivo* studies.

This chapter covers basics of ultrasound and the design, fabrication and characterization details for the following probes:

System 1: In-Vitro cell array system (small cm scale)- unfocused – Lower power- *in vitro* purposes

System 2: NDT Olympus V301 (large cm scale)- focused and unfocused – Lower power - *in vitro* and *in vivo* purposes

System 3: NDT Olympus V301 (large cm scale)- focused and unfocused - High power- *in vitro* and *in vivo purposes*

System 4: Probe AV2- In house fabricated (mm scale) - unfocused – Lowest power- *in vitro submerging purposes*

3.1.1 Acoustic Waves and Modes

Ultrasound is an oscillating sound pressure wave that is characterized by periodically high crests and low troughs that correspond to compression peaks and rarefaction minimums. These waves, generated by the source using oscillation or vibration, transfer energy from one point to another without the medium being transferred. However they stimulate the molecular bonds of a material by vibrating its particles about their resting position. Compression zones are regions where the molecular particles are close together, creating high pressure. Rarefactions are areas where the particles are far apart, creating low pressure.

Wave motion is described by distance and time parameters from one crest to the sequential one in terms of amplitude (Amp), wavelength (λ), period (*T*), Frequency (f) and wave propagation speed (c) (Figure 3-1).

One full cycle corresponds to one crest to the sequential one or one compression/rarefaction to the next. The wavelength (λ) is defined as the length of the space over

which one cycle occurs. Frequency (f) refers to the number of vibrations per second, measured in Hertz (1 Hz = 1 cycle/s) and is the ratio of the velocity of the wave traveling through a medium and its wavelength (λ). Sound wave travels at about 1500 m/s in fresh water at 25ºC.

$$f = \frac{c}{\lambda}$$

Equation 1 : Frequency

The time that takes for one cycle to occur is defined as the period and is the inverse of the frequency.

$$\tau = \frac{1}{f}$$

Equation 2 : Period

Ultrasonic pressure waves are longitudinal waves which travel parallel to the direction of motion. These waves are generated in two ways based on their temporal characteristics. Continuous sinusoidal waves (CW) are one of them which comprise of constant amplitude and have limitations due to the heating effects. Frequency (f), period (T), wavelength (λ), propagation speed (c) and amplitude (Amp) are sufficient to describe CW ultrasound. Cycles repeat indefinitely. The second type is pulsed wave (PW) that is a periodic repetition of few cycles of ultrasound (pulse duration) separated in time with gaps of no signal, hence it is non-thermal (Figure 3-2). PWs are used in imaging and therapeutic ultrasound and are described by their frequency (f), a specific number of cycles (N) per duration of pulse, the cycle time (T), pulse duration (PD) and pulse repetition frequency (PRF) which stands for the rate at which the duration repeats itself.

$$PD = N \times T = \frac{N}{f}$$

Equation 3 : Pulse Duration

Pulse repetition period is the time between the start of two successive pulse durations and is the inverse of PRF.

$$PRP = \frac{1}{PRF}$$

Equation 4 : Pulse Repetition Frequency

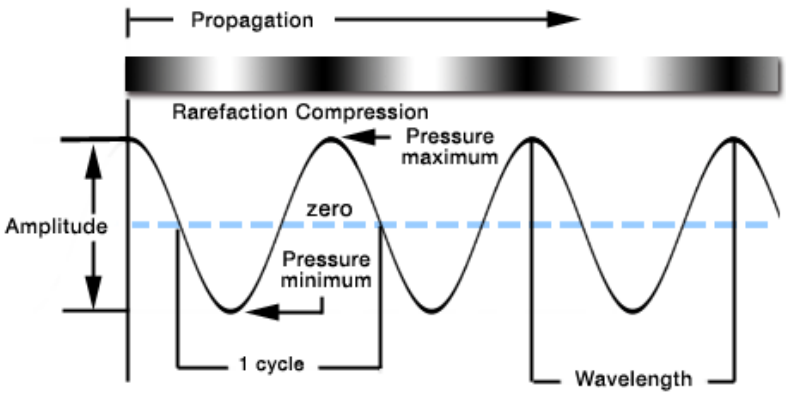

Figure 3-1 : Wave

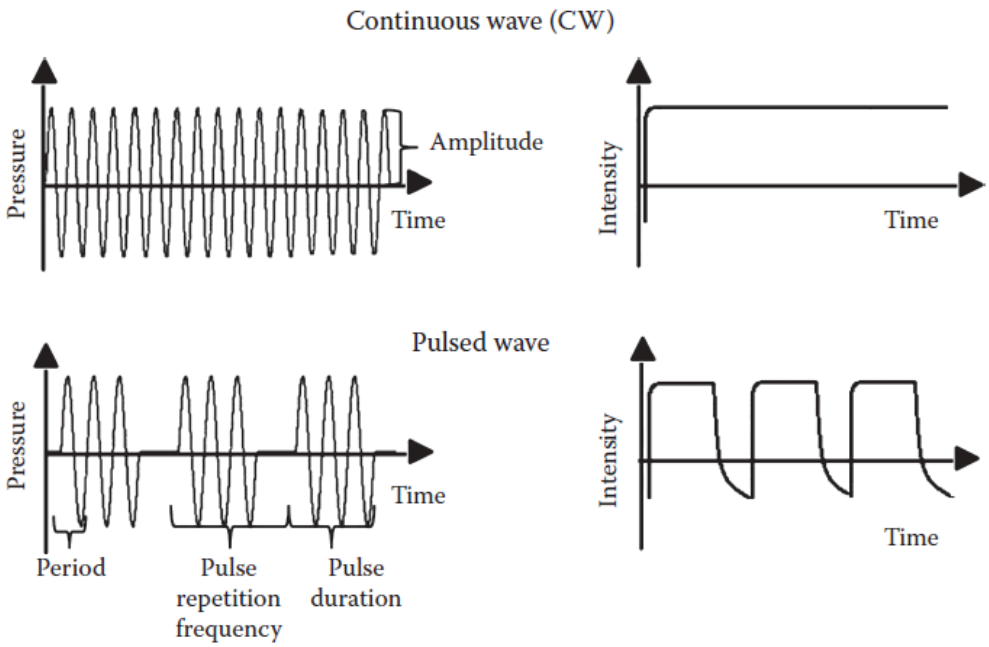

Figure 3-2: Graphical illustration of some of the critical parameters to vary the intensity and delivery of ultrasound energy, with a CW input (top) and a pulsed CW input (bottom) and corresponding intensity output profiles at the right.

The fraction of the time that the pulse is activated is called the duty factor (DF) or duty cycle (DC) presented in percentage.

$$\frac{DC}{100\%} = DF = \frac{PD}{PRP} = PD \times PRF$$

Equation 5 : Duty Cycle (DC) or Duty Factor (DF)

3.1.2 Acoustic Pressure

The acoustic pressure (P) is the change in total pressure at a given point. Amplitude of a wave is the maximum variation occurring in an acoustic variable and that Amplitude is measured in units of pressure. The simplified equation explaining the acoustic pressure waves in a medium with no attenuation traveling in one direction is as follows:

$$P = Po\sin(\omega t - kx)$$ Equation 6 : Acoustic Pressure Wave

Where ω is the angular frequency and *k* is the wave number.

$$\omega = 2\pi f$$ Equation 7 : Angular Frequency

$$k = \frac{2\pi}{\lambda}$$ Equation 8 : Wave Number

3.1.3 Acoustic Intensity, attenuation and impedance

Intensity is one of the key parameters used to characterize an ultrasound wave. Intensity is the rate at which energy density passes through unit area normal to the direction of propagation. An average intensity of a sound beam is the total power in the beam divided by the cross sectional area of the beam. The instantaneous intensity (I_i) and Average intensities (I) are mathematically defined as follows :

$$I_i = \frac{P_i^2}{\rho c}\ [\mathrm{W/cm^2}]$$ Equation 9 : Instantaneous Intensity

$$I = \frac{P_i^2}{2\rho c}\ [\mathrm{W/cm^2}]$$ Equation 10 : Average intensity

Intensity is important when referring to the bioeffects and safety. The intensity is proportional to square of the maximum amplitude (P), so if the amplitude is doubled the total intensity is quadrupled. Intensity Varies in focused ultrasound because it's highest at the center of the beam and falls off near the periphery. It also varies along direction of travel due to focusing and attenuation (Figure 3-3).

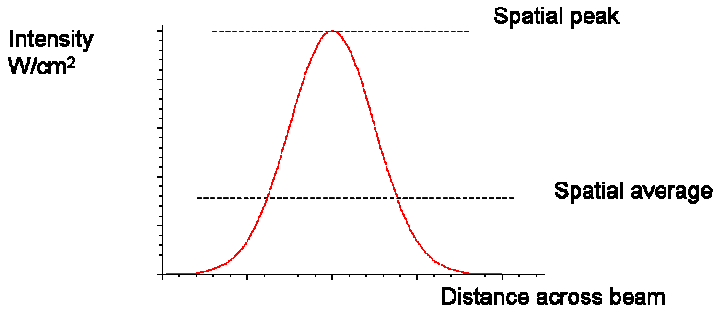

Figure 3-3: Intensity variation across beam

However, Intensity varies with time in pulsed ultrasound. It equals zero between pulses and not during the pulse duration (PD) (Figure 3-4).

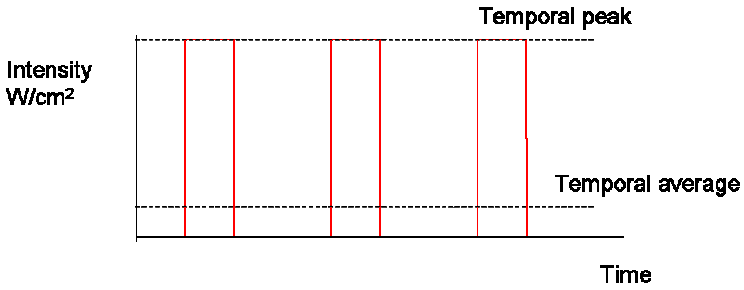

Figure 3-4: Intensity variation over time

Figure 3-5:Intensity measured based on location of the beam cross section

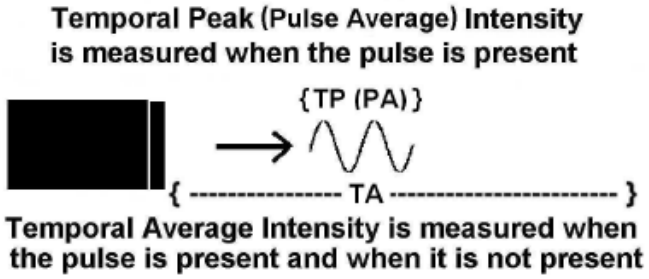

Figure 3-6: Intensity measured based on time

It's worth nothing that the ultrasound energies causing bioeffects are commonly reported using one of the six different types of intensities available. Many different methods may be used to measure the strength of a sound beam but before intensity measurements are performed, two decisions must be made. The first decision is, where in the beam's cross section will the measurement be made? The second decision is time dependent. When during Pulse wave will the measurement be made?

The highest Intensity found in a pulse is temporal peak intensity (I_{TP}). However, temporal average intensity (I_{TA}) is averaged over the pulse repetition period and is the lowest Intensity since it includes the time of the gap with no signal. Pulse average intensities (I_{PA}) is averaged over the pulsed duration and is in between I_{TP} and I_{TA}. I_{PA} and I_{TA} are related through the duty factor:

$$I_{TA} = I_{PA} \times DF$$

In case of a CW, I_{PA} and I_{TA} are equal. Combining these four spatial and temporal Intensities we end up with six intensities: spatial average-temporal average Intensity (I_{SATA}), spatial peak-temporal average intensity (I_{SPTA}), spatial average-pulse average Intensity (I_{SAPA}),

spatial peak-pulse average Intensity (I_{SPPA}), spatial average-temporal peak Intensity (I_{SATP}), and spatial peak-temporal peak Intensity (I_{SPTP})

Here is the order of the intensities from highest to lowest based on averaging in space or time or both:

$$I_{SPTP}(I_{SPPA})>I_{SATP}(I_{SAPA})>I_{SPTA}>I_{SATA}$$

In medical ultrasound, intensity is commonly measured at the spatial point of the highest intensity along the beam axis and is reported as either I_{SPPA} (intensity, spatial peak, pulse average) or I_{SPTA} (intensity, spatial peak, time average). I_{SPPA} measures the average intensity of each pulse and is a good indicator of mechanical bioeffects and cavitation, while I_{SPTA} provides a time-averaged intensity of all the delivered pulses and is generally an indicator of ultrasound-induced thermal effects (Fish 1990).

3.1.4 Attenuation

The ultrasound energy weakens as the waves propagate though the medium. This loss occurs based on two mechanisms as the wave encounters tissue interfaces. Those mechanisms are absorption (conversion to heat), and reflection and scattering.

Absorption is considered to be the main source of attenuation. As waves travel through a homogenous medium some of the energy convert into heat along the beam path due to absorption and that is identified by absorption coefficient $\alpha(f)$.$I=Ioe-2\alpha(^{f)x}$ Equation 11 shows the exponential attenuation of a propagating wave Intensity (I_o). This reduction is dependent on distance the beam travels, medium it travels through and finally the frequency (*f*). Attenuation is quantified in decibels (dB). The higher the frequency and the further the sound travels the higher the attenuation.

$$I=I_oe^{-2\alpha(f)x}$$ Equation 11 : Absorption Coefficient

$$\alpha_{dB} = \frac{10}{x}\log\left(\frac{I_0}{I(x)}\right)$$

$$\alpha_{dB} = \frac{20}{x}\log\left(\frac{p_0}{p(x)}\right)$$

Attenuation due to the reflection and scattering depends on the incident intensity at a boundary and the impedance of the mediums involved. The properties of each medium introduce resistance to the propagation of the waves. This resistance is dependent on the density and the speed of propagation in the specific medium. Impedance units are Rayls.

$$Z = \rho c \ [\text{Kg/m}^2\text{s}]$$ Equation 12 : Impedance

If the incident angle isn't perpendicular the medium the pressure amplitude reflection coefficient is calculated using the following equation:

$$R_P = \frac{P^r}{P^i} = \frac{Z_{0,2}\cos\theta_i - Z_{0,1}\cos\theta_t}{Z_{0,2}\cos\theta_i + Z_{0,1}\cos\theta_t}$$

Equation 13 : Pressure Amplitude Reflection Coefficient

Where P^r is reflected pressure at a medium interface, P^i is incident pressure, θ_i is incident angle and θ_t is transmission angle. In case of the normal incident the R_p *is:*

$$\left|R_P\right| = \frac{Z_2 - Z_1}{Z_2 + Z_1}$$

Equation 14 : Normal Incident Pressure Amplitude Reflection Coefficient

The loss due to the reflection will increase if there is a big mismatch between the impedance of the neighboring mediums. Transmission coefficient (T_P) for the amount of the Pressure that gets transmitted is:

$$T_P = 1 - R_P$$

Equation 15 : Transmission Coefficient

The intensity reflection and transmission coefficients, R_I, T_I, for a perpendicular incident are calculated using the following equations ($R_I = \left[\frac{Z_2 - Z_1}{Z_2 + Z_1}\right]^2$ Equation 16 and Equation 17):

$$R_I = \left[\frac{Z_2 - Z_1}{Z_2 + Z_1}\right]^2$$

Equation 16 : Intensity Reflection Coefficient

$$T_I = 1 - R_I = 1 - \left[\frac{Z_2 - Z_1}{Z_2 + Z_1}\right]^2 = \frac{4Z_1Z_2}{\left[Z_2 + Z\right]^2}$$

Equation 17 : Intensity Transmission Coefficients

The strengths of the reflected and transmitted pulses are determined by the impedances of the two media at the boundary.

If impedances are equal, there is no echo, transmitted intensity is equal to the incident intensity.

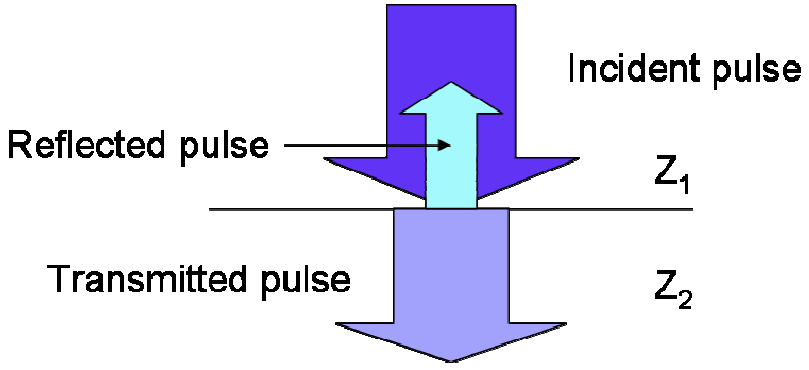

Figure 3-7:Impedance

3.1.5 Mechanical Index

While studying biological effects of ultrasound on tissues, a new parameter was discovered that is used to measure the cavitation. As mentioned earlier, basic mechanisms explaining bioeffects caused by the ultrasound energy are the heat (thermal) and cavitation/acoustic radiation force (mechanical). Heat is due to the friction produced as a result of vibration in tissue. Cavitation is the result of the production of gas bubbles in the tissue and possibility of nucleating inertial cavitation in worst case scenario. The cavitation formation depends on the intensity level of the therapeutic ultrasound. More stable cavitations are formed under low intensities of ultrasound and the effect of this type of cavitation is minor compared to the transient cavitations created during high intensities. Higher intensities may result in collapse of the bubbles and cause damage. Finally, safety indices were developed to predict the potential adverse bioeffects due to cavitation. The mechanical index (MI) value is based on the peak negative pressure (rarefaction) value divided by the square root of the radiation frequency of the transmitted ultrasound pulse:

$$MI = \frac{P_{peak\ -\ negative\ -\ pressure\ -\ in\ -\ MPa}}{\sqrt{f_{in\ -\ MHz}}}$$

Equation 18 : Mechanical Index (MI)

As the frequency decreases, the value for MI increases. US-FDA allows MI of up to 1.9 where no harm should be cause due to the peak acoustic pressure.

3.2 Design, Fabrication and Characterization of Ultrasound Probe

3.2.1 System 1: *in vitro* cell array system

To conduct *in vitro* studies and investigate molecular mechanism of action associated with ultrasound modulation, I fabricated, designed and characterized a cell array plate system. This cell array system was designed to accommodate a 96 well plate and for high throughput studies.

Our system is incorporated into a well plate that gives us the advantage to perform sonication studies per well rather than a full flask. The sonication is immediately followed by reading of ultrasound effect on cells and their ion channel flux behavior using fluorescent plate reader.

3.2.1.1 Methods & Materials

A cell culture experimental design was developed to investigate ultrasound stimulation on cell membrane and mechanosensitive properties of ion channels embedded in cell membrane.

Ultrasound array well Stimulator System

A well plate transducer array was engineered using 12 transducer elements with a 10 mm diameter (Figure 3-8). These elements were housed and sealed in a system designed to accommodate a well plate sitting above it. The array design avoided crosstalk between individual elements by complying with the necessary gap between the elements. The housing included the 12 transducer elements, a switch that turned the individual element on and off, and room for water coupling between each transducer and the bottom of the specific well being targeted. Coupling is necessary to avoid impedance mismatches in the ultrasonic path and to ensure correct beam propagation and focusing. The coupling system was designed such that the focused

ultrasound beam would pass through the aperture without distortion of the beam. Transducer elements were connected to a Miniamp (ZHL-32A, Minicircuits) powered by an Instek power supply (PST3201, Instek) and a function generator (33220A, Agilent) via the switch. The amplifier had a gain of 27 dB and a maximum power output of 1.66 W at 500 kHz. Each transducer was insonated using varying input power (up to 30dbm), PRF, DC and constant frequency of 1MHz. Please see the schematics for the complete system set up (Figure 3-9). The acoustic energy per individual element was measured with and without the placement of the well plate above the transducer array system.

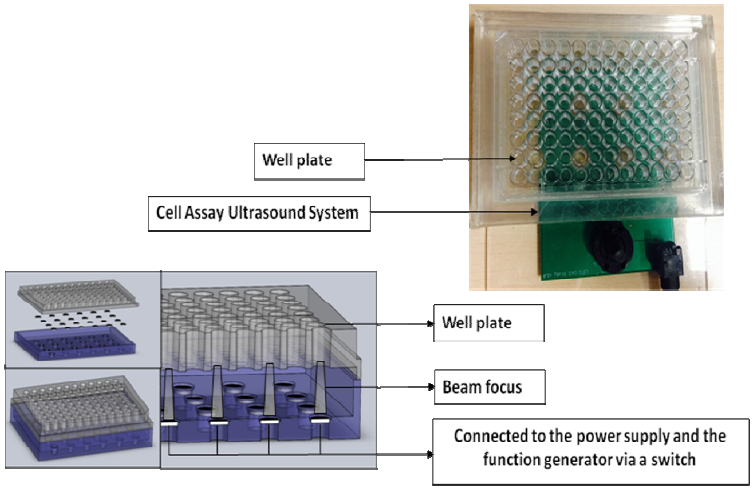

Figure 3-8: Transducer Array Well plate

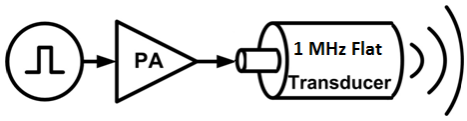

Figure 3-9: Schematics for cell array ultrasound system

3.2.1.2 Results and Analysis

The ultrasound beam measurement as well as resonant frequency per individual element was performed using a needle hydrophone (Onda Corp. HNR1000) submerged in the well filled with water. We observed no crosstalk between the individual elements. We also tested for acoustic reflection between the water and thin layer of the plastic on the bottom of the well plate. These readings showed no acoustic energy interruption by introducing the thin layer of well plate in between the hydrophone and the transducer.

In addition, the acoustic performance of the transducer and system were evaluated in a precision acoustic measurement tank (AIMS, Sonora/Unisyn, Longmont, CO) using the same calibrated needle hydrophone (Onda corp. Model HNR1000). These acoustic measurements are crucial because it enables us to measure the spatial and temporal distribution of acoustic pressures and the resulting intensity in a given medium. We obtained full width at half maximum (FWHM) (- 3 dB intensity, -6 dB pressure) curve of the acoustic field studied. It also allows us to compare our applied pressures and intensities in our specific studies to the rest of the experts in the field.

The following graphs are a summary of I_{SPTA} and pressure studies of one of the elements in the cell array system in the tank. The frequency of the transducer was kept constant at 1 MHz and PRF was kept at 1 KHz. Amplitude and the NOC were varied (50 & 200 (20% Duty cycle)). The results showed the linear effect of input voltage increase on both pressure and I_{SPTA}. However, the pressure stays almost the same regardless of increasing the when input voltage is kept constant. On the other hand the Intensity value varies by altering the DC linearly. As we raised the DC by 5 times our I_{SPTA} value increase by a factor of 5 as well.

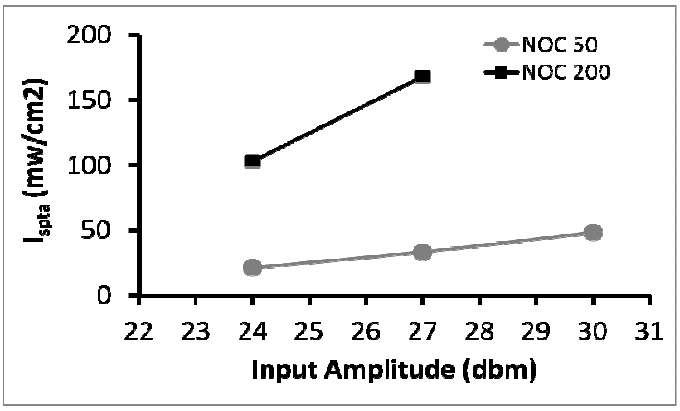

Figure 3-10: I_{SPTA} studies 0.5 cm distance from transducer surface- varying input amplitude and number of cycle (NOC) at a constant Freq of 1MHz

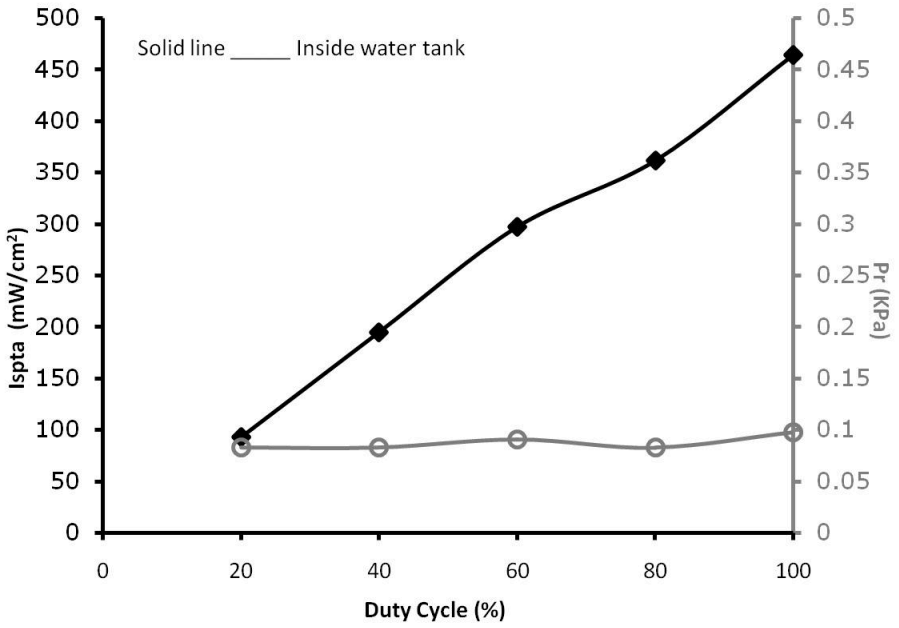

Figure 3-11: I_{SPTA} and Pressure studies at 0.5 cm distance from transducer surface-

A prototype for molecular ultrasound modulation studies was developed and integrated into a functional system. This system allowed us to focus within each individual well with 3dB spot size of 9mm in the well.

3.2.2 System 2: NDT Olympus V301 (*in vitro* studies)

To explore ultrasound frequency effect on modulation, system 2 was designed using a commercially available transducers that operates at 0.5 kHz. Olympus V301 is a commercially available transducer which comes in focused and not focused (flat) versions.

To conduct *in vitro* studies and investigate molecular mechanism of action associated with low intensity and low frequency ultrasound using these probes, I designed and characterized cell ultrasound system 2.

This system designed to accommodate culturing plates and well plates of different sizes.

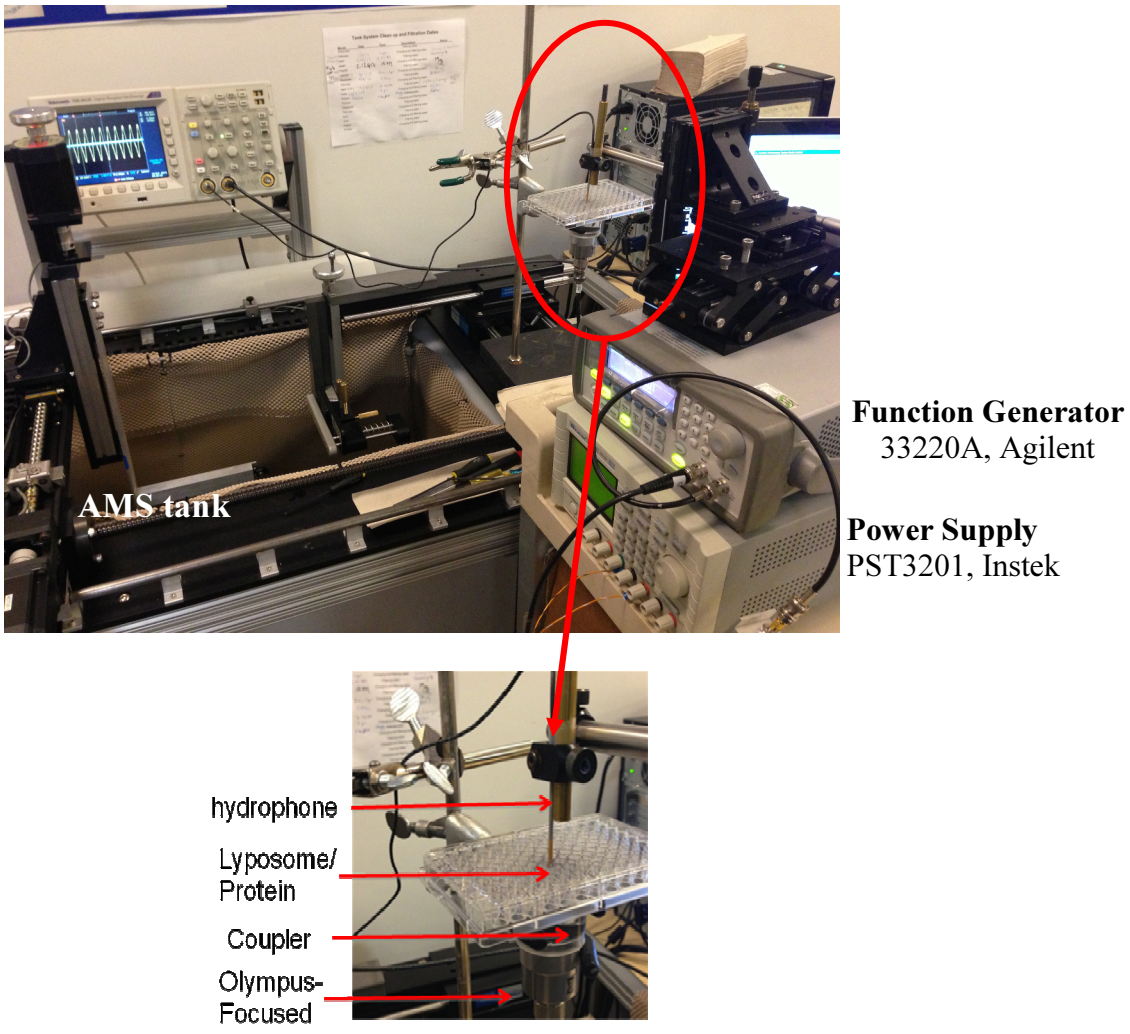

Figure 3-12: System 2 electronic and experimental set up using Olympus transducer - needle hydrophone submerged

3.2.2.1 Methods & Materials

Olympus V301 flat or focused probe:

The bottom of the plate was exposed to the transducer through a coupler. The coupler holds the appropriate amount of DI water and couples the bottom of the plate to the ultrasound irradiation. The coupler was a cylindrical PVC tube that created and sealed a water filled sonication chamber for the waves. The couplers height is chosen so the volume inside the well with cells are either at focus (for the focused plate) or in the far field for the flat Olympus transducer (Figure 3-12).

Transducer V301 (Olympus, MA) were connected to the same minicamp, power supply and function generator used in system 1. An electronic matching network (for better electronic coupling purposes) was used to couple the electronics to the transducer. Each transducer was insonated using varying input power (up to 30dbm), PRF, DC and constant frequency of 0.5MHz. Please see the schematics for the complete system set up (Figure 3-13). The acoustic energy per probe was measured with and without the placement of the plate above the transducer.

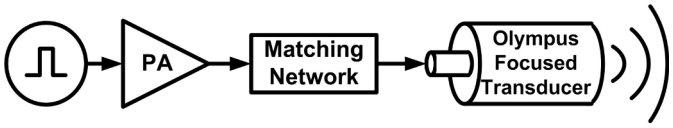

Figure 3-13: Schematics for Olympus focused/flat transducer

3.2.2.2 Results and Analysis

The ultrasound beam characterization was conducted using the same calibrated needle hydrophone (Onda Corp. HNR1000) submerged in the culturing plate/well filled with water as well as the tank (AIMS, Sonora/Unisyn, Longmont, CO) (Figure 3-12). This set up was

replicated during the experimentation. We left the hydrophone inside the well to mimic any acoustic reflection effect due to the hydrophone (Figure 3-14 dotted lines).

In addition, the acoustic performance of the transducer and system were evaluated in a precision acoustic measurement tank (AIMS, Sonora/Unisyn, Longmont, CO) using the same calibrated needle hydrophone (Onda corp. Model HNR1000) from System 1. The following graphs are a summary of I_{SPTA} and pressure studies of each transducer in the tank.

The frequency of the transducer was kept constant at 0.5 MHz, a and PRF was kept at1 KHz. Amplitude and the NOC were varied. The results showed the linear effect of amp input increase on both pressure and I_{SPTA}. Also, the pressure stays almost the same regardless of increasing the NOC due to the constant input voltage. On the other hand the Intensity value varies by altering the DC linearly. As we raised the DC, the I_{SPTA} value increases by the respective factor (Figure 3-14).

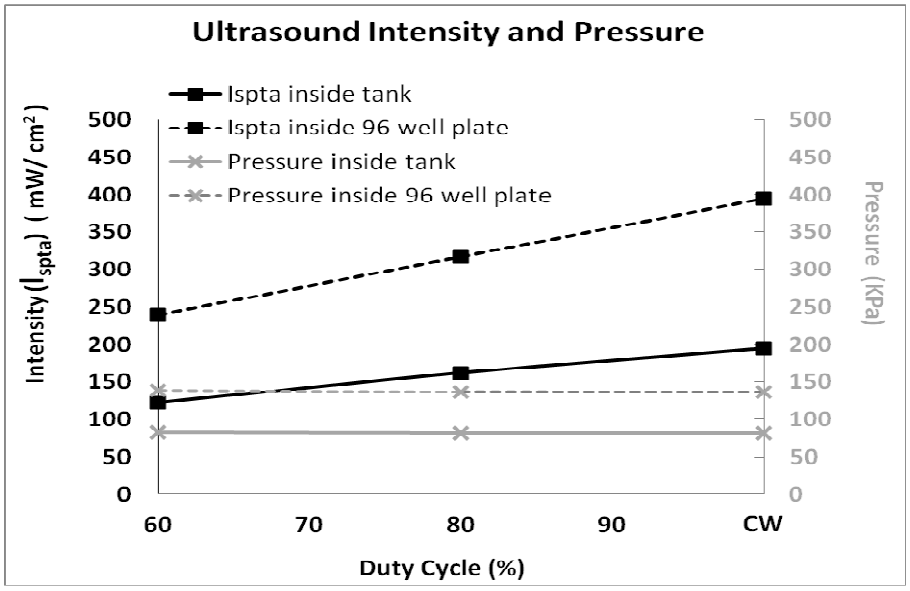

Figure 3-14: I_{SPTA} and Pressure studies at focus–
inside a 96 well (dotted values) and water tank (flat line)

We noticed a higher I_{SPTA} and pressure value when the measurements were performed inside the petri dish compared to the tank. The beam passes through the bottom of the petri

dish/plate and enters the small volume of the cell solution inside the well or the dish. The ultrasound wave experiences impedance mismatch leaving the surface of the solution inside the well which possibly causes reflections and contributes to the increase in intensity and pressure.

In addition, the hydrophone was submerged inside the small well volume for the beam characterization purposes. The metal inside the small and confined well volume causes reflections and increase in pressure and intensity values.

This system also enabled us to focus within each individual well and a parameter sweep was performed by varying DC, PRF and input amp.

3.2.3 System 3: Olympus V301 (*ex vivo* skull studies)

This system was used for the *ex vivo* studies. We used this system to conduct beam pattern deflection, reflection and attenuation studies introduced by a rat skull.

3.2.3.1 Methods & Materials

Olympus V301 focused probe:

The same commercially available transducers from system 2 was used for this set up. The focused transducer was used with a high-power drive system. System 3 schematics are shown in Figure 3-13. A computer controlled USB function generator signal was amplified using a Kalmus amplifier (1000HLMP-CE) The electronics were matched using the curved matching network just like our previous system (Figure 3-15).

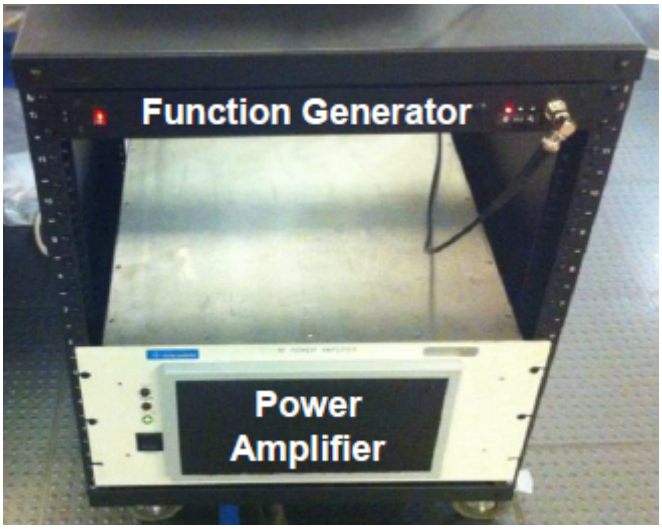

Figure 3-15: *ex vivo* skull electronics

3.2.3.2 Results

We characterized the system in 2 steps:

Step 1 - Electronic measurement: We conducted electronic measurement to learn about the voltage input limits into the transducer. We measured the output voltage waveform from the amplifier using Agilent DSO3202A oscilloscope, in response to a known input pulsed signal using the function generator. Some of the measurements were performed using attenuators with known values due to high input powers. Table 1 shows the relationship between the input voltage into the amplifier and the output value measure.

Step 2 – Acoustic measurement: Similar to the previous systems, we placed the focused transducer in the tank and conducted acoustic beam characterization at freq of 0.5 MHz, 1 KHz PRF, 0.02 volts input voltage and varied DC. The results are shown in Figure 3-16.

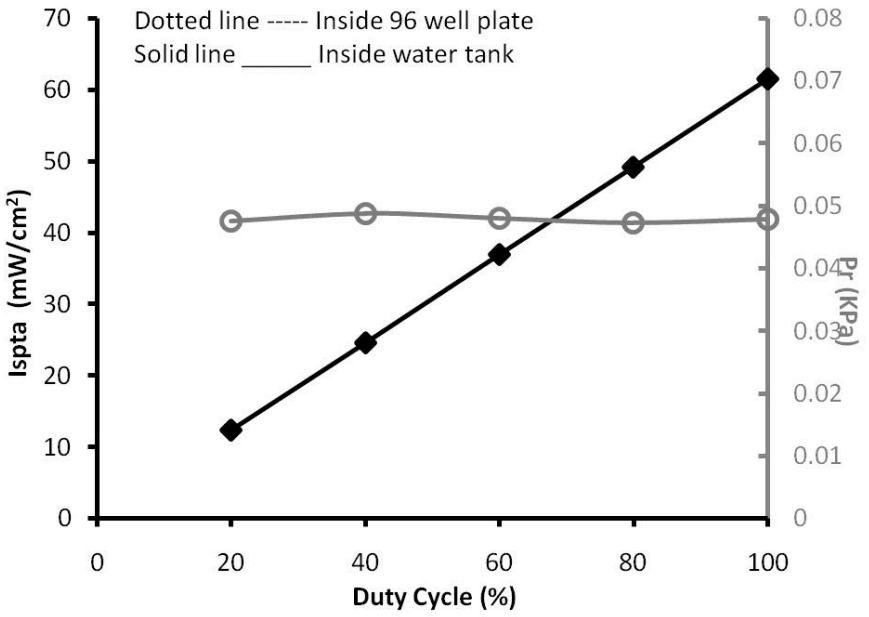

Figure 3-16 : *ex vivo* system characterization

		Duty Cycle	0.01	0.05	0.2
Vp-p in (before amp)	Vp-p in (v) (after amp)	Power - Peak (W)	Pavg (W)	Pavg (W)	Pavg (W)
0.02	14	0.501	0.00501	0.02505	0.1002
0.04	34.8	3.1	0.031	0.155	0.62
0.06	65.06	11	0.11	0.55	2.2

Table 1: Electronic characterization, Max power allowed = 0.125W

The table above highlights the limited list of the parameters that can be used by this system. The restrictions are due to the maximum power that can be applied to the focused transducer.

3.2.4 System 4: Miniprobe

This system was used for *in vitro* and invasive *in vivo* experiments. The probe was fabricated small enough to afford invasive surgeries in a rat model. In addition it was made compatible to a culturing well plate and a patch clamp system.

There was no coupling method needed for this system since the probe was made to be submerged directly in the solution volume. Figure 3-17 and Figure 3-18 show the electronics and the probe with its set up for the *in vitro* studies in relation to a well plate.

Amplifier
ZHL-32A, Minicircuits

Function Generator
33220A, Agilent

Power Supply
PST3201, Instek

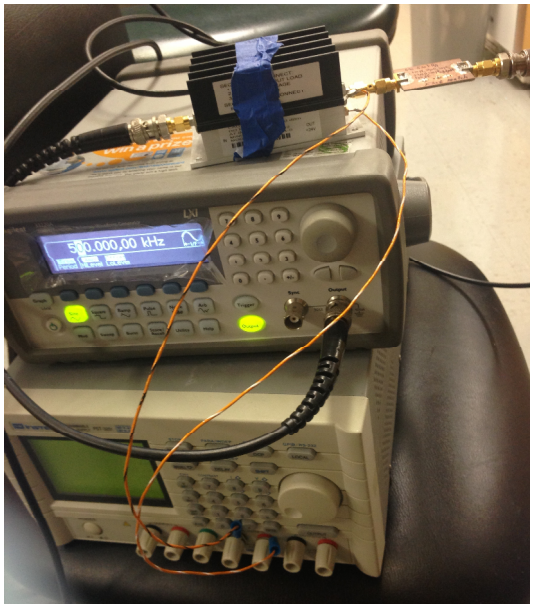

Matching Network
Custom made

Figure 3-17: Miniprobe electronics system for *in vitro* studies

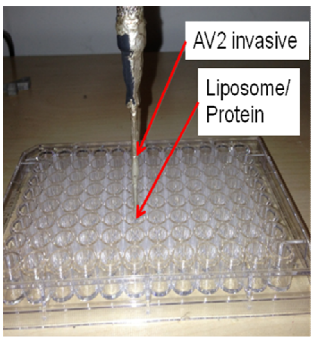

Figure 3-18 : Miniprobe and set up with respect to a well plate

3.2.4.1 Methods & Materials

In house fabricated unfocused probe:

This system is composed of an in house fabricated probe that operates at frequency of 0.525 MHz. The electronics powering this probe were similar to what was used in system 2.

The generated waveform was amplified using a Minicircuits amplifier (ZHL-32A) (gain of 27 dB) powered by an Instek power supply (PST3201). The amplified electronic waveforms were matched to the cable and transducer system using an electronic matching network. Miniprobe was sonicated using varying input voltage (up to 30dbm), PRF, DC and constant frequency of 0.525 MHz. The schematic for the complete system set up is shown in Figure 3-13. The acoustic energy was characterized inside the tank.

3.2.4.2 Results and Analysis

The acoustic performance of the miniprobe and system were evaluated in the tank (AIMS, Sonora/Unisyn, Longmont, CO) using the same calibrated needle hydrophone (Onda corp. Model HNR1000) as before. The following graphs are a summary of I_{SPTA} and pressure studies of miniprobe (Figure 3-19 and Figure 3-20).

The frequency of the transducer was kept constant at 0.5 MHz and PRF was kept at1 KHz. Amplitude (Figure 3-20) and the DC (Figure 3-19) were varied. The results showed the linear effect of amp input increase on both pressure and I_{SPTA}. We see a similar trend to the previous systems. The pressure stays almost the same regardless of DC increase. On the other hand the Intensity value varies by altering the DC linearly as we raised the DC (Figure 3-19). Also the I_{SPTA} and pressure value increase as we increased input amplitude (Figure 3-20).

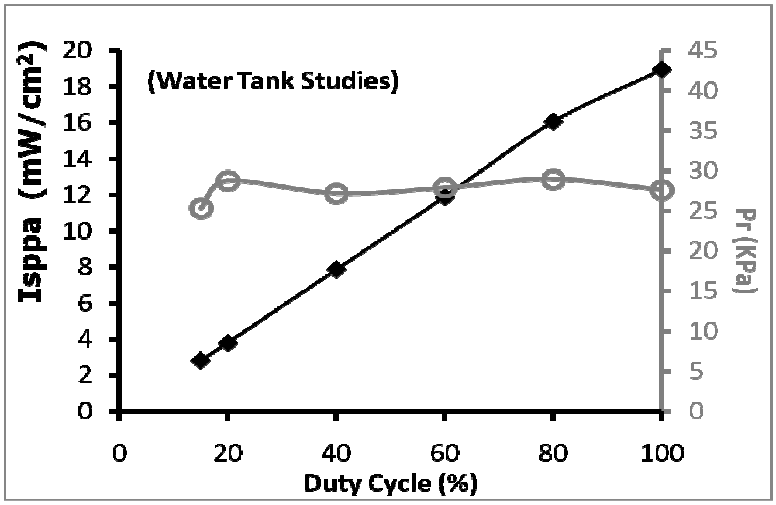

Figure 3-19: Miniprobe I_{SPTA} and Pressure, 0.5 cm away from transducer surface

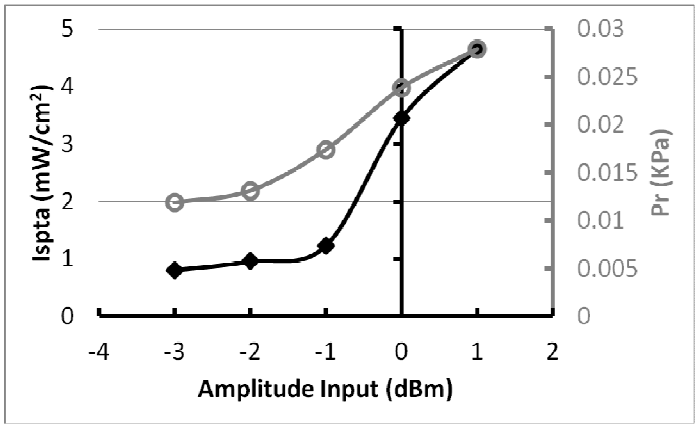

Figure 3-20: Miniprobe I_{SPTA} and Pressure, 0.5 cm away from transducer surface

This system enabled us to directly submerge the AV2 probe inside the well and sonicate the cells by sweeping through parameters. The characterization was performed in the tank and not inside a well. The size of the well didn't allow for more realistic measurement. Miniprobe sonication inside the well could experience reflections from the bottom of the plate but we won't be able to replicate that specific set up with the hydrophone. These reflections could raise the value of I_{SPTA} and pressures measured in Figure 3-19.

4 Mechanism of Action Associated with Low Intensity Focused Ultrasound Through MscL Protein Mechanosensitive Channels

4.1 Abstract

Recent in vivo modulation of region-specific brain activity suggests that Low Intensity Focused Ultrasound (LIFU) may be a non-invasive alternative therapy for drug-delivery applications and the treatment of neurological diseases such as epilepsy and Parkinson's disease. Despite the recent in vivo success, the underlying mechanism explaining LIFU neuromodulation remains unknown. It is thought that mechanical perturbation of neuronal cellular membranes, or proteins embedded in these membranes, has an impact on ion channel kinetics leading to depolarization, and ultimately, increased potential discharge.

We have established a simplified in vitro model to test the non-cavitational hypothesis of LIFU neuromodulation using large conductive mechanosensitive channels (MscL), and non-mechanosensitive channels, NaK2K and KVAP, reconstituted in membrane vesicles. We report that ultrasound modulation and membrane perturbation induces membrane protein-lipid dependent pore formation rather than gating the channels. However at high mechanosensitive channel concentrations, a dual effect of membrane stretch enhancement in the membrane and decreased pore formation was noticed upon focused ultrasound stimulation.

4.2 Introduction

Treatments for neurological and psychiatric disease such as Alzheimer, Parkinson's and epilepsy, and neuropathic pain management are currently limited to pharmacologic or invasive surgical strategies. While pharmacologic treatments can be designed to target specific neurotransmitters, they lack the regional selectivity that device interventions often times attempt

to leverage. In addition, there can be adverse effects associated with the pharmaceuticals as well as concerns about drug metabolism and clearance in individuals with compromised hepatic and renal function [60]. Conversely, neurosurgical interventions such as resections and Deep Brain Stimulator (DBS) that is now an established clinical procedure and in clinical studies for multiple neurological applications, can target specific region of brain. However these methods are considered invasive and have an associated morbidity risk [1, 5, 61]. Novel transcranial magnetic stimulation has the advantage of being completely noninvasive, but lacks spatial resolution and the ability to focus on deep brain structures [62]. Thus, there appears to be an acute need for an affordable, non-invasive neuromodulation intervention that can target deep brain structures.

To address these limitations, there has been an increased interest in using focused ultrasound (FUS) as a strategy for noninvasive neuromodulation.

Ultrasound-induced bioeffects were identified as early as 1929 showing *ex vivo* muscle contraction using high intensity ultrasound parameters [63]. However, ultrasound application as both suppressive and reversible neural activator wasn't explored until 1950s [23, 64]. These findings were further investigated via many *ex vivo,* small and large animal models. For example, a few *in vitro* studies revealed that FUS can effectively stimulate both neurons in culture and a short-latency excitatory response in a rodent brain-slice assay [12, 46]. Tyler demonstrated that low-intensity (pulse average intensity < 3 W/cm2) and low-frequency (440 and 670 kHz) ultrasound pulses can induce reproducible excitation of neuronal circuits in *ex vivo* mouse hippocampal neurons. Later, Tyler and his colleagues performed *in vivo* studies on an intact mouse brain targeting the hippocampus using unfocused transducers which caused motor activity [11, 12]. In a separate murine investigation, effective regional modulation was generated using intensities of 1.6-6.3 W/cm^2 and frequencies as high as 650 kHz. These parameters

resulted in stimulation of neurons, while the same study revealed suppression of motor activity at 160 mW/cm^2, suggesting a bimodal effect dependant on intensity [47]. A similar bimodal effect was seen in rats, where higher intensity stimulation, 4.6 W/cm^2 at 350 kHz, stimulated cranial nerves [48]. Finally, a study evaluating the efficacy of continuous versus pulsed sonication in a murine model concluded that either mode can be effective in neuromodulatory stimulation [8]. Ultrasound stimulation studies in conjunction with function magnetic resonance imaging (MRI) by Yoo and his colleagues revealed both stimulation and suppression of a rabbit cortex activity as well [47]. More recent studies demonstrated the feasibility of saccade modulation in the awake nonhuman primate brain [65].

Thus, there appears to be compelling *in vivo* evidence of the neuromodulatory capabilities of FUS, leading investigators to believe that FUS may be a candidate for transcranial neuromodulation for conditions such as Parkinson's disease and Epilepsy. Despite these successful studies, there exist important gaps in the current knowledge that must be bridged to advance the field. 1- The mechanism underlying the FUS neuromodulation is unknown and 2- the parameters that successfully stimulate, or suppress, nervous activity are obscured by the vastly different experimental and systemic protocols used in these studies.

in vitro Hypothesis : Currently, the prevailing hypothesis explaining the adiabatic neuromodulatory capacity of focused ultrasound suggests that pressure transmitted to the tissue creates alteration of the lipid membrane due to its elastic characteristics, causing modulation of protein channels and mechanoreceptors embedded within the membrane. This modulation of protein channels is then thought to have some effect on cellular excitability, action potential variation, and neurotransmitter release or uptake [12, 49]. Debate continues on whether the increased pressure transmission is generated due to the formation and collapse of gaseous

cavitation bubbles [8], or due to a non-cavitation mechanisms resulting from acoustic radiation propagating through the tissue [14]. Regardless, both sources of pressure are thought to modulate ion-channel kinetics, leading to depolarization, and ultimately to increased action potential discharge [13]. Prior studies indicate that many voltage-gated ion channels show mechanosensitive properties that render their gating kinetics sensitive to transient changes in lipid bilayer tension [11]. Moreover, researchers have shown that ultrasonic exposure to fibroblasts in culture can induce a reversible increase in intracellular Ca^{2+} concentration, thereby supporting the hypothesis that ultrasound is modulating ion channel gating [13]. Finally, previous work investigating the effect of focused ultrasound on ionic conductance using a fluorescent dye in individual neurons revealed activation of voltage-gated Na^{+} and Ca^{2+} channels, altering the membrane potential and initiating nerve conduction [12]. Thus, several studies suggest that protein channel modulation is possible using a variety of focused ultrasound systems and parameters but no conclusive results have verified yet.

We carried out the following studies to investigate the adiabatic and non-cavitational hypothesis underlying low intensity focused ultrasound (LIFU) stimulation using a simplified proteoliposome model. This simplified model does not take the cellular exoskeleton and other structures into consideration to focus studies only on the protein and liposome interaction. Our liposomes include the Large-Conductance Mechanosensitive Channel (MscL), one of the best characterized mechanosensitive (MS) channels, and two non-mechanosensitive protein channels. We also evaluated different acoustic intensities for future effective *in vivo* applications.

As mentioned earlier, MS protein channels seem to be membrane tension gated. Many studies have shown that the biophysical properties of the membrane, especially tension within the membrane, can be sensed by MS proteins as well as microbial sensors and pumps [66, 67].

For example, *E. coli* MscL channels have been used in multiple studies to investigate the protein-lipid interaction and how lipids induce conformation responses onto proteins. To test this interaction, Moe and Blount reconstituted MscL into a definite lipid systems and activated it by pressure gradient. The channels activation was due to the tension transmitted directly through the bilayer and not because of membrane curvature or the pressure across the membrane [68, 69]. In addition, MscL has the largest opening among the bacterial channels which allows big molecule and small protein efflux through its pore. Thus, the effects of membrane tension on protein confirmation are exaggerated and easier to study by physiological and biophysical means. These properties make MscL a great paradigm for investigating the mechanical influence of low intensity and low frequency ultrasound on cells and structural changes at the molecules level.

Our results confirm Tyler's hypothesis of spring-like mechanism of protein channels, and Krasovitski's membrane stretch and contraction introduced by ultrasound modulation in a simulation model in response to LIFU stimulation using 500 kHz frequency. Surprisingly we noticed a decrease in flux at higher MscL protein concentrations of the embedded mechanosensitive protein channels, thus supporting a "spandex" hypothesis proposed by Boucher *et al.* [70]). Also, our studies of intensity and duty cycle agreed with King's *in vivo* results where continuous waves are more effective than pulsed ultrasound. These finding offer a new understanding of the LIFU mechanism and ultrasound parameter space for future effective *in vivo* applications and for higher repeatability rate and successful ultrasound stimulation.

4.3 Materials & Methods

4.3.1 Experimental Models

Four sets of proteoliposome models were used to study the effect of focused ultrasound on ion channel gating and membrane tension. These simplified *in vitro* models have the

advantage over living cell models in the aspect that data could be interpreted without the complication of the effect of other cell components. The first control model was composed of liposomes with no protein channels. The next two control models, NaK2K and KVAP, were non-selective cation channels reconstituted in liposomes that have not reported to be gated by mechanical stimuli. Finally, we used MscL as our MS model to compare ultrasound effects on mechanical sensitive channels to non-mechanical sensitive channels and no channel models.

4.3.2 MscL and Bilayer Interaction upon Gating

The bacterial Large-Conductance Mechanosensitive Channels (MscL) is one of the best characterized MS channels. MscL is located in the cytoplasmic membrane of most bacteria [71], where it plays a vital role in osmoregulation by protecting the cell from lysis upon acute decreases in external osmotic environment by releasing cytoplasmic osmolytes [72], thus serving as a biological "emergency release valve". MscL is gated directly by membrane stretch or tension transmitted directly through the bilayer [68], and it lacks ion selectivity. When there is no osmotic downshock and no tension is felt by the membrane, the channel is closed. Upon gating, the channel pore expands and the opening is about 30 Å. Because of these properties, as well as its tractable nature, MscL presents an excellent model for studying how a channel can sense and respond to biophysical changes in a lipid bilayer introduced by ultrasound.

4.3.3 *Liposome Formation, Protein Channel Reconstitution and Calcein dye loading*

The protocol for MscL purification [68] and reconstitution [73] was established through Dr. Paul Blount's lab [74, 75]. The protocol is illustrated in Figure 4-1. The lipid used composed of 1,2-Dioleoyl-sn-glycero-3-Phosphatidylcholine (DOPC), cholesterol and 1,2-distearoyl-sn-glycero-3-phosphoethanolamine-N-[amino(polyethylene glycol)-2000 (DSPE-PEG 2000). To quantify the LIFU effect on protein membrane interaction, calcein (a fluorescent dye) efflux

assay was used. Calcein dye self-quenches at high concentrations but fluoresces at lower concentrations, i.e. if it is fluxed out of the loaded liposomes. This calcein assay allowed on-site detection of changes in liposome membrane permeability upon ultrasound stimulation.

Lipids (DOPC/Cholestrol/DSPE-PEG 2000 in a molar ratio of 70/20/10) were dried and rehydrated with 50 mM calcein to form liposomes, which were then saturated with Triton-X100 and mixed with purified protein channels. The reconstitution of protein channel was completed upon removal of the detergent by Bio-Beads^{TM} SM-2 adsorbent (Bio-RAD) and separation of proteoliposome from the free calcein was performed by running the sample through size exclusion column.

We extended our studies by evaluating the effect of different protein concentrations on ultrasound-induced changes in membrane permeability. The liposomes had different tolerances for the three channels tested, beyond which the liposomes yield was drastically reduced. Channels were reconstituted into liposomes to the maximum feasible concentration possible per channel type. We then diluted the protein amounts to 1/2, 1/4 and 1/8 of the highest concentration per protein channel and reconstituted them in vesicles. This protein concentration range allowed us to observe the effect of channel concentrations on membrane permeability induced by ultrasound.

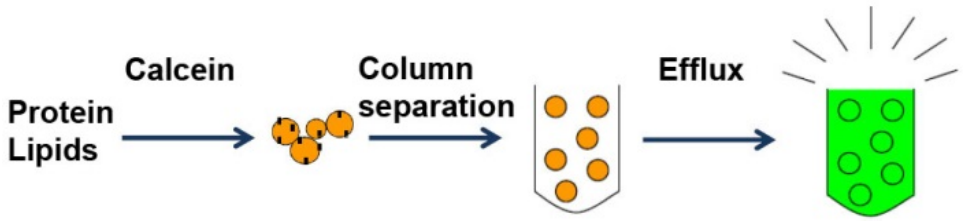

Figure 4-1 : An illustration of proteoliposome preparation procedure

4.3.4 Verification of the Presence of the Protein Channel

To confirm protein channel presence and their gating behavior in liposomes, we treated proteoliposomes with lysophosphocholine (LPC), a functional assay, besides ultrasound, that has been reported to gate MscL by changing the membrane tension profile surrounding the channel protein (Perozo 2002). The fluorescent signal was monitored for 5min and 30 min before and after LPC treatment, which was followed by a 5 min signal measurement after lysing liposomes by 0.5% Triton-X 100. All signals were normalized to the value after Triton treatment. In liposomes reconstituted with MscL, NaK2K or KVAP channels treatment with LPC at concentration of 125uM led to calcein efflux and increased fluorescent signal. The specificity of this effect is confirmed by the fact that no apparent fluorescent signal change was observed in vesicles without MscL, NaK2K and KVAP (Figure 4-3). This is a practical system to verify the presence of the mechanosensitive protein channels and their channel activity. However, the non-mechanosensitive channels (NaK2K and KVAP) were not expected to efflux since there is no report of these channels being sensitive to mechanical stimuli, and the calcein dye size is too large for the open pore size of these channels, which will be further discussed in the results section. Regardless, these results clearly indicate the influences of the membrane protein channels in the lipid bilayers as higher effluxes are dependent upon higher protein concentrations.

4.3.5 Ultrasound System & Set Up

To investigate the mechanism underlying ultrasound stimulation we used system 2 from chapter 3. Our system was made of commercially available focused transducers used for non-destructive testing (NDT) purposes (V301, U8423001, Olympus). This system was designed to accommodate culturing plates and well plates of different sizes (Figure 3-12).

The bottom of the plate was exposed to the transducer through a coupler. The coupler was a cylindrical PVC tube that created and sealed a water filled sonication chamber for the ultrasound irradiation. The coupler's height was chosen so the volume inside the well with cells was at the focus of the transducer (Figure 3-12).

A sinusoidal waveform was generated using a function generator (33220A, Agilent) and it was amplified using a Minicircuit's amplifier (ZHL-32A, Minicircuit) powered by an Instek power supply (PST3201, Instek). The signal was electronically coupled using a matching network to the focused transducer (Figure 3-13). The amplifier had a gain of 27 dB. The frequency of the transducer was kept constant at 0.5 MHz, PRF was kept at1 KHz, NOC and voltage input were both varied. However, only the highest voltage resulted in sufficient results and they are being reported here.

4.3.6 *Acoustic Beam Characterization*

The ultrasound beam characterization was conducted using a needle hydrophone (Onda Corp. HNR1000) submerged in the culturing well plate solution. The arrangement of the well plate with respect to transducer mimicked the experimental set up. The hydrophone submersion inside the well was replicated during the experimentation to imitate any acoustic reflection effect due to the hydrophone during the acoustic characterization (Figure 3-12).

In addition, the acoustic performance of the transducer and system were evaluated in a precision acoustic measurement tank (AIMS, Sonora/Unisyn, Longmont, CO) using the same calibrated needle hydrophone (Onda corp. Model HNR1000). As mentioned before, voltage input and frequency were kept constant and the intensity was varied by changing duty cycle (DC) per pulse. Figure 4-2 summaries I_{SPTA} and pressure values collected in the tank (flat line) and inside the well plate (dotted line) per Duty Cycle.

The results showed that regardless of increasing the NOC the pressure stayed constant at around 83 kPa when measured inside the tank and 140 kPa inside the well plate. On the other hand the Intensity value varies by altering the DC linearly. As we raised the DC from 60% to continuous wave (CW), the I_{SPTA} value increases from 122 mW/cm2 to 194 mW/cm2 inside the tank and 240 mW/cm2 to 394 mW/cm2 inside the well plate (Figure 4-2). Therefore we noticed a higher I_{SPTA} and pressure value when the measurements were performed inside the well plate compared to the tank.

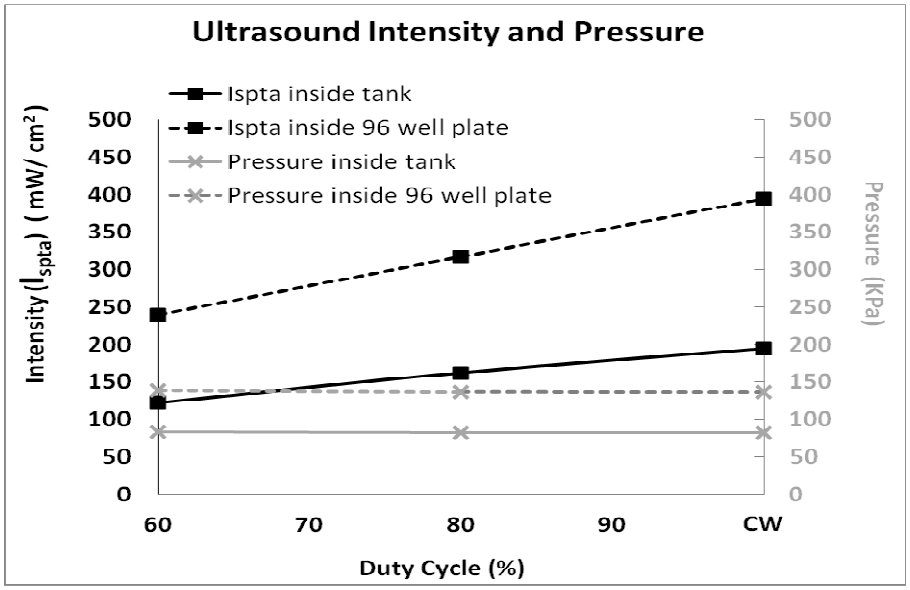

Figure 4-2 : I_{SPTA} and Pressure studies at focus inside a 96 well plate (dotted values) and water tank (flat line)

We also studied the effect of duration of insonation on the MscL protein membrane interaction. We varied duration from 5 min to 20 min in increments of 5. Duration of 5 minutes didn't show much of an efflux so we didn't continue our studies. We compare results from 10 min to 20 min LIFU sonication of MscL-liposome vs. liposome only models.

4.3.7 Experimental Protocol

As mentioned before, the set up included the transducer that was coupled to the bottom of a 96 well plate via DI water. Appropriate volume of vesicle or proteoliposome was added to vesicle buffer to achieve final volume of 200 μL in 2 wells of clear bottom 96-well plates and attain similar vesicle count and fluorescent signal after Triton X-100 treatment in each well among studies. One well was kept as a control and the other one was exposed to LIFU from the bottom of the plate well. The wells were chosen to be at least 5-6 well distances from each other to avoid cross talk. Baseline fluorescence was recorded for both control and ultrasound treated samples prior to insonation at 538 nm with the excitation at 485 nm using a Fluoroskan Ascent plate reader (Thermo Scientific Inc., Waltham, MA, USA). Next, the sample wells were treated with ultrasound in room temperature for 10 min or 20 min using the parameters mentioned above. Lower intensities and durations less than 10 min were explored and didn't reflect much difference in results between the control and proteoliposome models. Therefore we focused on insonation of 10 min and 20 min duration, and the 60%, 80% and CW DC parameter sets. In addition, temperature was monitored before and after each sonication. The absence of air bubbles was confirmed inside the coupler and the wells. To replicate the acoustic characterization set up environment inside the well plate, a hydrophone was submerged inside the well during sonication. Fluorescent was measured after ultrasound modulation using the same plate reader. Finally vesicles were lysed at the end by adding 10 μl of 10% Triton X-100 to determine the total released fluorescence levels. All signals were normalized to the values after Triton treatment. The data collected was analyzed statistically using MATLAB. Paired *t*-test comparison between fluorescence levels of vesicles as a function of treatment/concentration were performed per day due to the variation of results per treatment from day to day. The

statistical significance p-value is presented as followed: *: $p < 0.05$, **: $p < 0.01$; ***: $p < 0.001$; ****: $p < 0.0001$

4.4 Results & Discussion

Four *in vitro* models were stimulated using our ultrasound system to test the protein channel gating hypothesis of mechanism underlying LIFU modulation. The wells with no ultrasound exposure resulted in zero efflux.

4.4.1 LPC Induced Calcein Efflux From Liposomes Reconstituted With Protein Channels

The results from the LPC functional assay test are illustrated in Figure 4-3. This graph is a summary of all 3 *in vitro* models and their varying protein concentration reconstitutes. LPC has previously been used to gate the MscL channel [76]. LPC induced calcein efflux was therefore attempted to be used as an indication of channel presence and activity of mechanosensitive channels. We observed significant amount of MscL calcein efflux after LPC treatment, as expected (Wilcoxon matched-pairs signed rank test, p-value = 0.001). In addition, as MscL protein concentration increased the LPC induced calcein efflux increased accordingly. However, we were surprised to find a similar trend with the non-mechanically activated channels, as efflux percentage rose significantly in KVAP and NaK2K channel models (paired *t*-test, p-value varies per protein concentration) (Figure 4-3). Further note that the size of KVAP and NaK2K channel opening isn't large enough to allow passage of calcein. These data strongly suggest that calcein is fluxed by a mechanism independent of channel gating, perhaps some sort of pore formation at the lipid-channel interface. Regardless, these results clearly indicate the influences of the membrane protein channels in the lipid bilayers as higher effluxes are dependent upon higher protein concentrations.

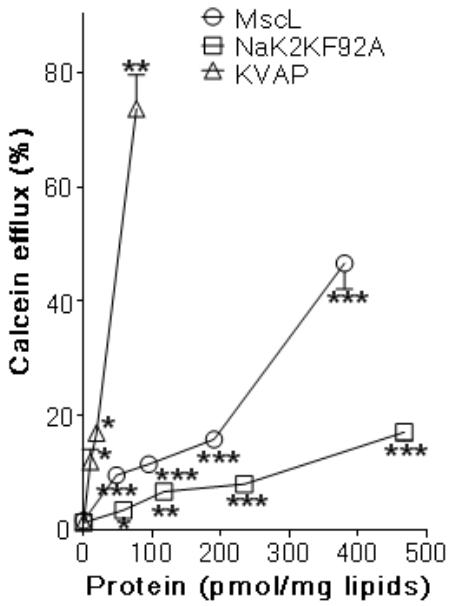

Figure 4-3 : LPC induced calcein efflux from liposomes reconstituted with protein channels

4.4.2 Proteoliposome Stimulation Using LIFU Pulsation vs. Continuous Wave

To understand the effect of different intensities on the protein and lipid interaction, we varied our pulse DC from 60% to a CW. We applied 500 kHz frequency and input voltage of 30 dBm to Vesicle-control, MscL and NaK2K proteoliposome suspension. For this set of experiments, the protein concentration was kept constant at the highest pmol per model for simplicity purposes (MscL 380 pmol/mg_ lipids and NaK2k 467 pmol/mg_lipids). MscL and NaK2K channels were statistically tested with respect to the control vesicles within the same DC group. Paired *t*-test compared the values from the same day to each other, since our results varied from one day to next. In conclusion, our duty cycle study results agree with King's *in vivo* findings [8] as each liposome type showed higher efflux as we went from pulsed wave to the continuous wave.

Also regardless of the DC, a consistent increase trend was noticed in MscL channels compared to its control vesicles, but yet did not achieve statistical significance. Where as in the NaK2K model, a significant efflux increase was measured compared to its control vesicle in both the 80% DC and CW cases (paired *t*-test, p-value =< 0.05). This could be due to better MscL channel stretch capabilities compared to the non-mechanosensitive channels stretch properties..

In addition, the incremental efflux drop reveals that lower acoustic intensities have less membrane modulation effect which is noticed in 60% DC. There was no significant efflux variation detected amongst the samples while using 60% DC. The efflux gap between the test samples and the control is the most exaggerated at the higher DCs. Therefore, we chose to continue our studies using CW.

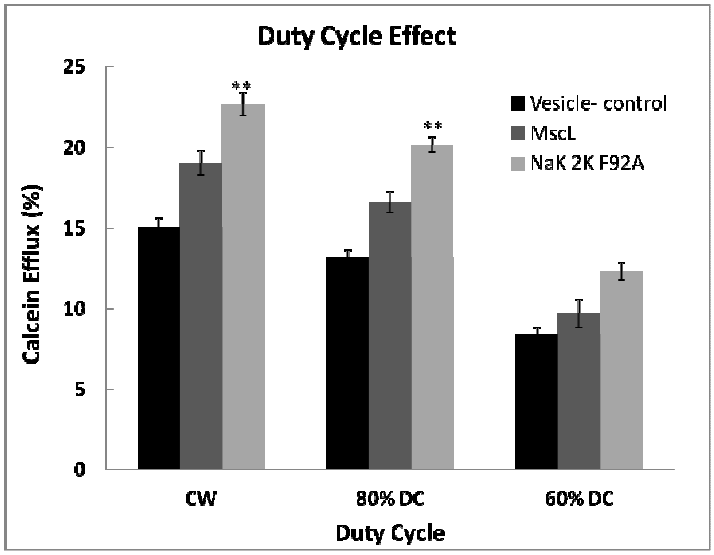

Figure 4-4 :LIFU stimulation duty cycle effect studies

4.4.3 Protein Concentration Effect on Proteoliposome Stimulation Using LIFU

To better understand the effect of LIFU on the protein-membrane modulation, we extended our studies to varying protein concentration per sample. All four models were

insonated using CW from this point on. We kept the frequency at 500 KHz, voltage input at 30 dBm, applied a CW and stimulated each well for 10 minutes. Different protein concentrations in each model were statistically compared to the calcein efflux of the control vesicle model. The vesicle model had the lowest efflux percentage compared to the other three proteoliposome (containing MscL, NaK2K and KVAP). Also, the insonation results revealed efflux percentage increases for all three proteoliposome sets as the protein concentration increased. This increase was considered statistically significant for some of the protein concentration as indicated in **Error! Reference source not found.**. We were surprised to find that only in the MscL channel group, the efflux percentage significantly dropped at the highest protein concentration level compared to the lower MscL concentrations except the no-protein control. Paired *t*-test analysis results are presented in Figure 4-5.

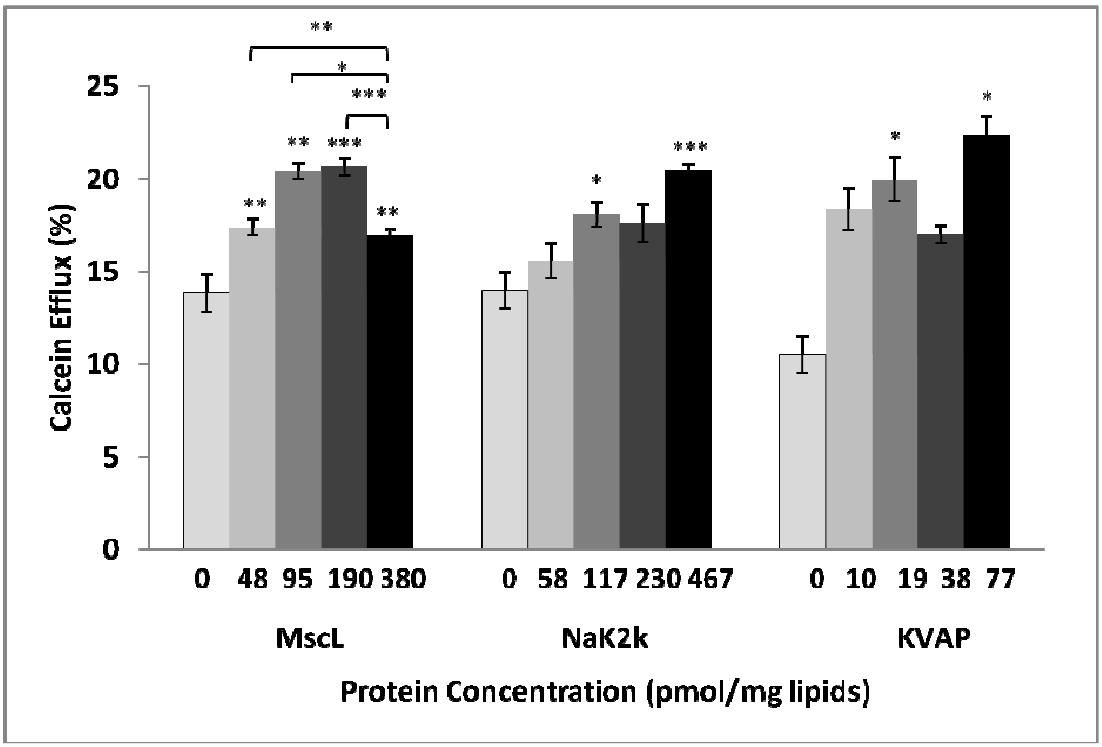

Figure 4-5 : Calcein Efflux Against Protein Concentration

Since the efflux isn't selective, meaning all three models resulted in an efflux increase as protein concentration increased, we concluded that calcein efflux wasn't through the protein channel pores, and instead it was presumably through pores formed either in the membrane or at the channel-liposome interface, as speculated for the LPC-induced efflux, above. However, the efflux decrease at the highest concentration of MscL channel, unlike the non-mechanically stimulated channels, could reflect a spandex effect proposed by Boucher [70].

Boucher explored how MS protein channels with stretch abilities, also called membrane "spandex", can maintain bilayer tension within a particular range by closed-closed expansion. His two state (expanded/contracted) simulated model was inspired and designed based on characteristics and expression levels of bacterial osmovalves and its values, specifically MscL channels. The model tested the closed-closed expansion en route to opening, or preopen expansion states in the activation path(8), and overexpression in the bacteria which act as stretch gated tension buffers to avoid unnecessary opening of osmovalves. MscL preopening expansion transition has been predicted to expand as far as 80% its open area prior to gating [77].

Initially isolated proteins were characterized within a membrane. Later the model composed of a population of MscL proteins to study the effect of the protein concentration on the membrane behavior. The model revealed that 1- the spandex area can expand to a specific limit, in the plane of the bilayer, prior to transition to its open state. This activation barrier was found to be crucial. 2- As the concentration of the spandex protein channels increased, higher amount of imposed strain was endured by the membrane prior to achieving the transition of the channels (Figure 4-6). 3- The spandex protein expands to alleviate the tension in the membrane when the tension exceeds a certain level and contracts in case of decrease in tension. This behavior will dampen the tension introduced on the membrane. The goal is to maintain a constant tension in

the membrane even if the imposed strained varies as seen in Figure 4-6Bii, the flat section. These results require a larger protein area expansion rather than smaller one. In addition to the protein area expansion, higher concentrations of proteins with even very small area expansion can behave as tension-damping spandex proteins.

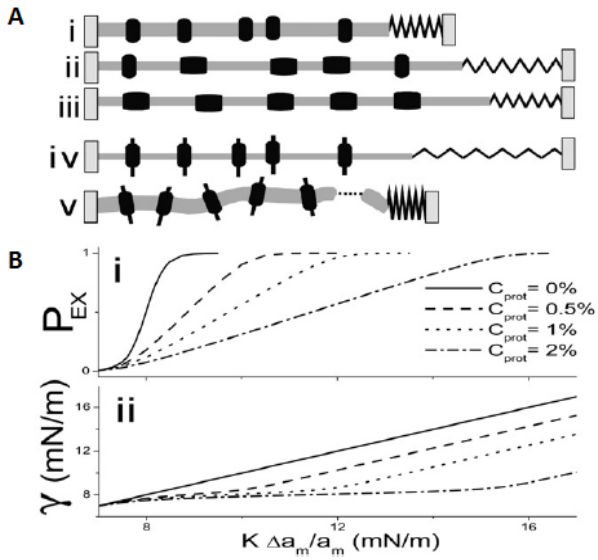

(A) A mildly stressed membrane with contracted spandex proteins (i) that is suddenly exposed to a large strain (due, say, to high turgor) (ii) will experience elevated bilayer tension (the spring length, γ, increases) that progressively falls as more spandex proteins expand (iii). If the membrane contained exclusively nonexpansible proteins (iv) it would be more likely to rupture (v).

(B) The effect of spandex protein channel concentration, Cprot, on PEX (i) of , and on γ (ii), as a function of imposed strain multiplied by bilayer compressibility: $K\Delta a_m/a_m$). (i) Shows the PEX midpoint right-shifting and (ii) shows bilayer tension flattening with increasing Cprot.

PEX _ probability for a protein to be in the EX state

Cprot_protein concentration

Figure 4-6 : Boucher's spandex membrane tension model [70]

Therefore, in our studies, the spandex effect could explain the MscL channel's extra stretch ability that gives this proteoliposome conformation higher tolerance to the acoustic stimulation compared to the non-mechanically stimulated channels. Finally our results provide the first experimental evidences for Boucher's model of mechanically stimulated channels using LIFU as a stimulus.

4.4.4 LIFU Duration effect on Proteoliposome Stimulation

As we focused on the CW, we also investigated the LIFU stimulation duration effect on the membrane modulation and permeability. We used control vesicles and highest MscL protein concentration model (380 pmol/ mg_lipids) for this set of studies. Our results showed significant

decrease in efflux from Vesicles (p-value = 0.01) and an insignificant decrease in efflux in MscL models as the duration of LIFU stimulation was lowered from 20 min to 10 min. This reveals increased membrane perturbation or pore formation due to longer period of insonation (Figure 4-7).

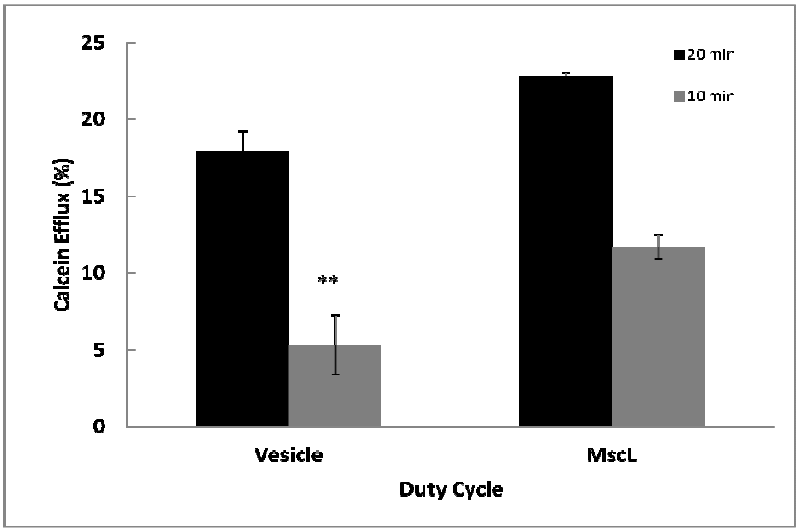

Figure 4-7: LIFU stimulation duration effect studies

4.4.5 Discussion and Conclusion

Several *in vitro* and *in vivo* studies have revealed effective ultrasound stimulation of nervous tissue resulting in measurable stimulation of action potentials, as well as, measurable electrophysiological outcomes. Despite these recent results, success rates remains low, in part, due to a knowledge gap around the mechanism underlying stimulation and the missing data exploring the ultrasound parameter space that causes stimulation. To address this gap we explored the adiabatic and non-cavitational mechanism of LIFU insonation using a simplified *in vitro* proteoliposome model and narrowed down our studies to a specific LIFU parameter set.

Our results reveal that for all treatments, ultrasound acoustic intensity increases efflux, suggesting an effect of focused ultrasound on membrane permeability regardless of the type of membrane protein. However, at a certain concentration, the inclusion of MscL channels into liposomes reacted differently to the LIFU stimulation when compared to the non-mechanically stimulated protein channels. The highest concentration of MscL showed a reduction in efflux signal compared to its half protein concentration treatment. This suggests that, contrary to the dogma in the field, we have no evidence that any of our protein channels are gated by focused ultrasound stimulation at these experimental conditions. These results imply that focused ultrasound is having an effect on the permeability of the membrane itself or, because it shows a dependence of the concentration of membrane protein incorporated into the liposomes, at the channel-lipid interface.

Our results agree with Krasovitski's proteoliposome simulation model called "bilayer sonophore" (BLS) that explains the cellular membrane's ability to absorb LIFU mechanical energy and transforming it into expansions and contraction of the intramembrane space. The BLS simulation model showed that extremity of the bio-effect on the cell membrane depends on different ultrasound parameters exposure and maximum area strain ability of the leaflets. The bio-effects may vary from delicate and reversible excitation of the cell membrane to pore formation and even damage to membrane proteins and/or cytoskeletal fibers [49].

We observed pore formation in all three models. However, an enhanced membrane stretch effect was observed only in the MscL case and only at the highest protein concentration level (380 pmol/ mg_lipids). This observation reflects a dual effect of pore formation and the enhanced membrane stretch effect when studying mechanosensitive MscL channels, and thus also agrees with Boucher's "spandex" effect in which the protein expands within the membrane,

increasing its external radius. As noted in Boucher's model, the mechanosensitive channels can dampen the acoustic energy transformation onto the intramembrane spacing by stretching and slow membrane tension relief. This highlights the significance of the specific MscL protein concentration necessary to allow slow tension relief instead of pore formation. The lower MscL concentrations and the non-mechanically stimulated proteins channels presumably weren't able to stretch enough to protect the proteoliposomes while they were being mechanically perturbed by LIFU acoustics. It also appears that this enhanced membrane stretch effect is not possible with non-mechanically stimulated channels since they do not expand within the plane of the membrane as much as MscL channels.

In addition, our study of parameters reflected results similar to King's *in vitro* studies [8]. We observed that CW has stronger effect on the protein membrane perturbation compared to pulsed acoustic parameters per sample channel which holds true with King's studies. Thus the longer our samples were exposed to LIFU acoustics, the higher protein membrane perturbation was observed. Our results suggest a new understanding of mechanism that explains ultrasound stimulation. Our experimental results and future *in vitro* studies expanding to more complex cell models including cytoskeleton hopefully will offer future researchers the knowledge necessary to determine the applicability and capabilities of LIFU-stimulated neuromodulation that will further the ongoing research into treatment for diseases such as epilepsy, Parkinson's disease, and chronic pain.

5 Acoustic Characterization of Low Intensity Focused Ultrasound System through Skull

5.1 Introduction

The focus point and intensity of LIFU through the skull of small animals has not been studied in depth, due to the assumption that the skull size and dimensions are small enough that can be ignored. This however has been recently proven to be a poor assumption by this work and others. This work has investigated the skulls impact on targeting and energy delivery in addition to enhancing our understanding of the molecular mechanism underlying neuromodulation using focused ultrasound. To improve future transcranial, non-invasive neuromodulation outcomes, investigation of the skull's impact on targeting accuracy, and energy attenuation is necessary for clinical translation of this technology. As mentioned earlier, low ultrasound frequencies are more favorable in transcranial ultrasound stimulation due to lower acoustic beam attenuation and aberration through skull bone. However low frequency and low attenuation result in higher standing waves, especially in small animal skulls due to reflection from the bottom of the skull. Despite this disadvantage, majority of the noninvasive transcranial LIFU *in vivo* studies have been conducted using rodents where the skull cavity is small enough that acoustic standing waves can occur depending on the parameters used. Azuma *et al.* was able to demonstrate and compare the standing wave formation inside the skull by 500 kHz and 2 MHz ultrasounds using Schleren imaging [78]. Later, O'Reilly and Hynynen measured standing waves in 2 *ex vivo* rat skulls using a hydrophone inserted inside the skull cavity through a hole in the skull base [79]. They varied frequency and target inside the skull cavity, and studied the effect on standing waves and general focal shift per frequency in two rat skulls. They learned that standing wave patterns were detected in rodents tested and it can be eliminated using a wideband composite sharply focused transducer and a reduced duty cycle. Also, they noticed that as the

frequency increased the ultrasound focus inside the skull shifted away from the transducer. However they did not measure exact focal shift for a specific target location or study the remaining space inside the cavity beside the focal axis [79]. Younan and Aubry tried addressing beam profile in the entire head through simulation and *in vivo* experiments to investigate the *in situ* pressure and intensity level as well as the spatial pressure distribution. They repeated their *in vivo* acoustic parameters through simulations and reported that the acoustic field was spread over the whole rat brain with the presence of several secondary pressure peaks [80]. These studies have demonstrated what is considered safe and effective parameter space for non-invasive transcranial focused ultrasound, and simulated the beam distribution within the skull cavity.

An *ex vivo* rat skull model has been used in our studies to explore the focal shift, reverberation, and attenuation for a specific target deep inside the skull cavity, hypothalamus. A pulsed waveform with a low frequency, low duty cycle and low intensity was used to avoid standing waves and excess attenuation. These *ex vivo* studies will characterize the precise energy deposition and beam deformation of focused ultrasound to improve our ability to compensate for the effects of the skull, and therefore enhance *in vivo* targeting for future studies.

5.2 Materials & Methods

5.2.1 Acoustic energy measurements without skull

"System 3: Olympus V301 (*ex vivo* skull studies)" discussed in Chapter 3 was used to study the effect of the *ex vivo* rat skull on the ultrasound focus point. Trials were conducted using a commercially available focused ultrasound probe (V301, U8423001, Olympus). This focused ultrasound transducer was used with a high-power drive system. The generated waveform was amplified using a Kalmus amplifier (1000HLMP-CE). The output of the amplifier was matched to the probe using a matching network to maximize the energy transfer to the transducer. The

transducer was operated at its resonant frequency, for maximum efficiency, of 0.5 MHz, 1 kHz pulse repetition frequency (PRF), 20% duty cycle (DC) and 0.02 volts peak-to-peak input amplitude (Figure 5-1).

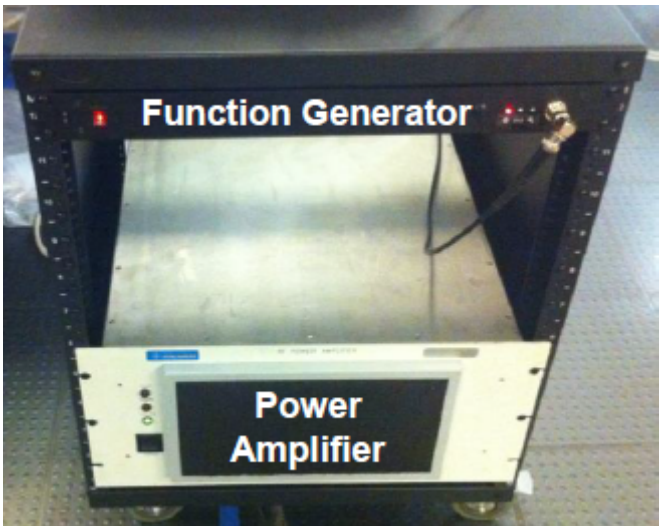

Figure 5-1 : *ex vivo* skull electronics

The acoustic performance of the Olympus focused transducer V301-SU with and without the skull specimen was evaluated inside a precision acoustic measurement system (AMS) tank (Acertara Acoustic Laboratories, Longmont, CO) (Figure 5-2) using a calibrated needle hydrophone (Onda Corp. Model HNR1000). The AMS is a precision scanning system mounted on a water tank that allows measuring and mapping of acoustic fields, including imaging and therapeutic devices, between 250 kHz and 60 MHz. The bottom of the tank, walls and the hydrophone holder were all lined with rubber padding to absorb reflections inside the tank as much as possible. The scanning system consists of a three axis positioning system that holds the hydrophone. The hydrohphone communicates with the AMS software on a PC through an oscilloscope. The data collected through the AMS software was extracted and analyzed via MATLAB (Mathworks, MA, USA). These acoustic measurements enabled us to measure the

spatial and temporal distribution of acoustic pressures and intensities, and calculated the Full width at half maximum (FWHM) (- 3 dB intensity, -6 dB pressure) curve of the acoustic field studied.

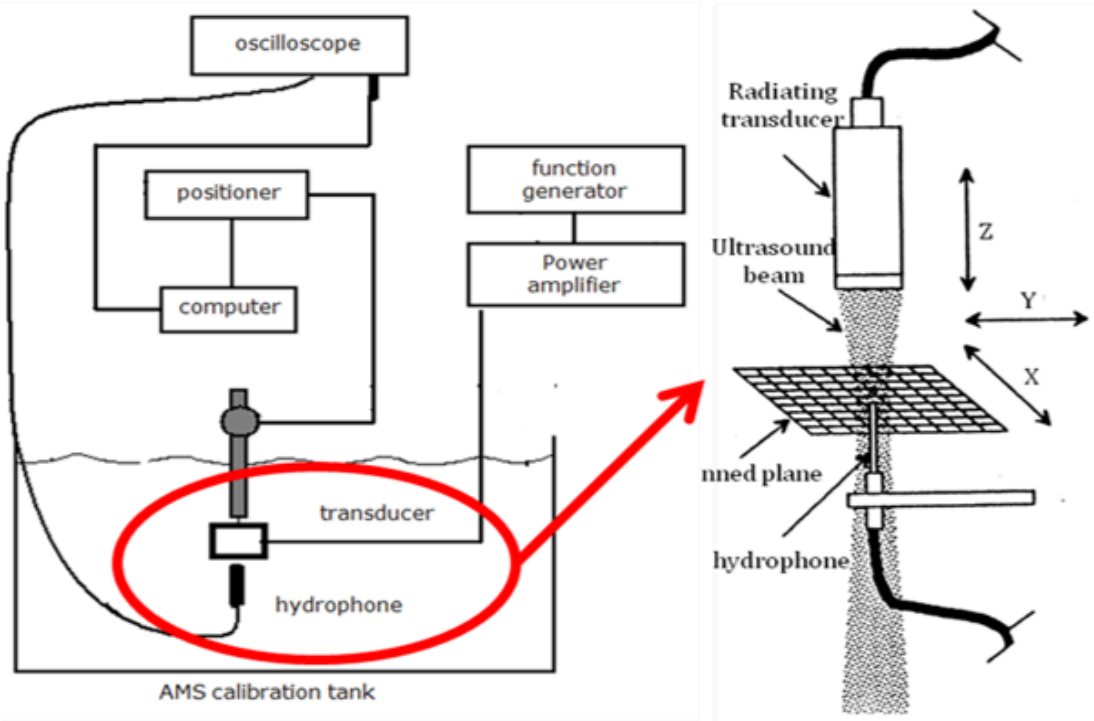

Figure 5-2 : Acoustic measurement system tank (AMS)

Initially the transducer was incorporated into the tank without the skull presence (**Error! Reference source not found.**). With the transducer stationary and the hydrophone scanning the acoustic field, the focus of the transducer with it's appropriate I_{spta}, pressure, and beam shape were recorded by cross axis scan, z-scan at the focal axis at increments of 0.2 mm, and finally raster scans at focal plane, before and after focal plane.

Our acoustic characterization results of the probe reflected about 12 mW/cm^2 I_{spta} and about 40 kPa acoustic pressure at the focal point. Beam focal zone measured as 2 mm in height and about 3 mm in diameter (Figure 5-3).

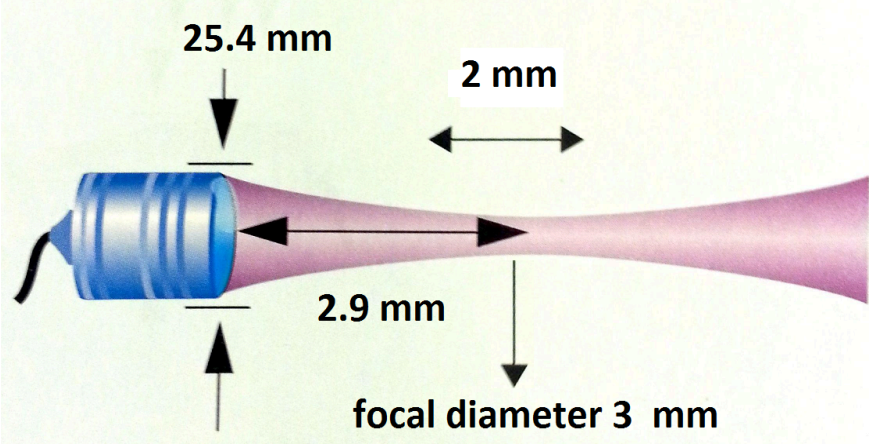

Figure 5-3 : Beam focus shape

5.2.2 Skull preparation and alignment with respect to the tank set up

Nine *ex vivo* rat skulls were obtained from sprague dawley (SD) rat cadavers with an average weight of 180-220 grams. The lower mandibles were removed and the rest was skeletonized by manual dissection of the flesh followed by subsequent exposure to a dermestid beetle colony. The top of the skull was measured to have a thickness of 1mm to 1.25 mm . A 2 mm diameter hole was drilled through the skull base, stopping at the interior wall of the top of the skull. The location of the hole was aligned with the coronal axis of our target of interest in the brain. Efforts were made to replicate the *in vivo* set up for the ultrasound delivery to the hypothalamus from our previous experiments. Based on the skull dimensions and the transducer focal point measurements from the previous steps, we attached the skull to a submersible fixture and mounted the fixture to the transducer sitting inside the AMS tank in a way where the focus of the transducer fell within the skull at 2.8 mm inferior from the bregma targeting the hypothalamus (Figure 5-4 and Figure 5-5).

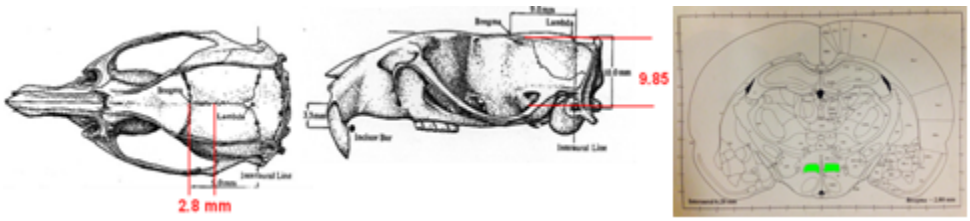

Figure 5-4 : Target inside rat skull

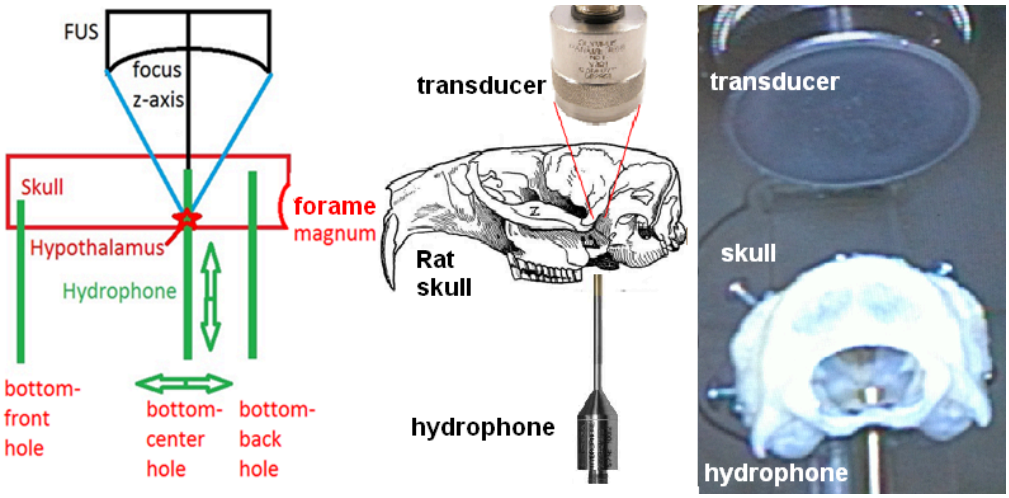

Figure 5-5 : (left) Full rat skull schematic with three inferior holes, (middle & right) Photograph of hydrophone, skull, and transducer placement

The transducer was kept stationary during this attachment process and its previous position with respect to hydrophone was preserved. The skull cavity was flushed with DI water to ensure no bubbles were trapped in any of the cavities

At this point, the skull specimen was situated in the water tank with the focused ultrasound transducer positioned at the top exterior of the skull held stationary using a manual positioning stage. The hydrophone was mounted on the XYZ scanning stage positioned at the bottom exterior of the skull specimen (Figure 5-5).

Two additional holes were made at the base of 5 skulls. The first was near to the nasals and the second was close to the foramen magnum. The purpose of these two additional holes was to study reverberation away from the focal point and axis (Figure 5-5).

5.2.3 Beam characterization inside a full skull

Beam propagation, focus, and intensity map was measured within the brain cavity along the focal axis by scanning the transducer relative to the hydrophone with the skull in between (Figure 5-5). A full skull cavity study was performed in the following manner:

1. To measure the focal shift, we inserted the hydrophone inside the skull cavity through the 2 mm center hole and conducted z-axis scan at 0.2 mm interval. Z-scan started from beneath the top of the skull until 2 cm post-focal and along the acoustic focal axis.
2. To study the effect of the skull orientation with respect to the transducer. We repeated the z-scan three times for each skull (n=7) by completely detaching the fixture holding the skull from the transducer mount and reattached it.
3. The hydrophone was inserted through the two non-focal axis holes at the skull base to measure reverberation. Acoustic properties from front and back of the skulls were recorded and compared to the focal axis hole acoustic pressure and intensities(Figure 5-5).

5.2.4 Beam characterization with top half of skull

After completion of the full skull studies, the skulls were bisected axially ("half skull"), and the first two steps from full skull study were repeated using the hydrophone and the top half of the skull only (Figure 5-6). In addition to focal shift and reverberation, we conducted raster scans at focal point, and pre- and post- focal point to determine the planar contour of the acoustic beam. A window of 30 mm x 30 mm was chosen for the raster scan to cover the beam at focus and the data collected was normalized to the highest focal pressure at the center. This data revealed the beam deformation and focal shift in the transverse plane caused by the top half of the skull.

The results from the full and half skull will allow us to compensate for the focal shift and deformation caused by skull properties, skull orientation with respect to the transducer, and reverberation inside the skull cavity for future *in vivo* studies.

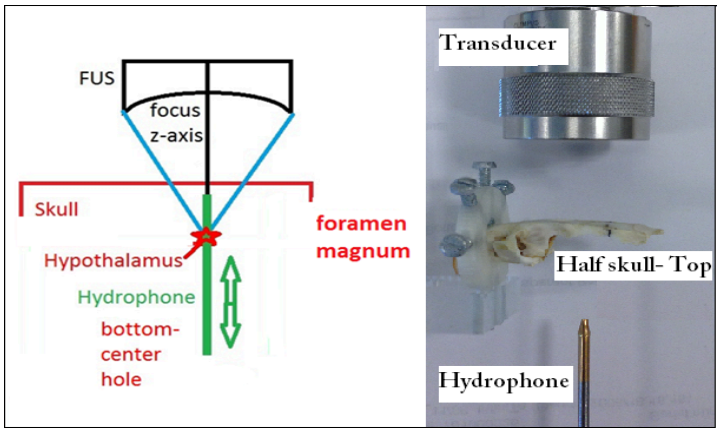

Figure 5-6 : (left) Half rat skull diagram. (right) Visible photograph of half rat skull setup

5.3 Results and Discussion

To prepare for *in vivo* efficacy studies, the ultrasound beam scattering and focal shift that occurs as ultrasound passes through the skull was characterized using the effective parameters found from prior *in vivo* studies. This will allow us to optimize our focused ultrasound beam and the associated parameters to achieve a higher success rate of neuromodulation in pre-clinical (proposed *in vivo* rat studies), and ultimately clinical, models.

During our studies, we used one point target inside the skull cavity and one set of parameters. Oreilly *et al.* studied different frequencies, different target points and 50% DC vs. CW effects on standing waves in *ex vivo* full rat skulls but never explored the transverse motion of the target using half skull and he didn't report on the exact focal shift [79]. We measured the focal shift introduced by the skull both in the coronal and transverse plane in addition to measuring reverberation. In addition, the acoustic target and beam deflection with and without

the skull, reverberation inside the skull cavity, skull orientation effect with respect to the transducer and finally attenuation due to the skull was characterized during our experiments.

Initially we examined the coronal focal shift in a full skull and later, the focal shift in the transverse plane using only the top half of the same skull. Preliminary data from nine rat skulls revealed that beam intensity, beam shape, and targeting are all significantly affected during transcranial stimulation.

Our data from full skull and half skull studies showed that the beam shape is deformed by the presence of the skull, with the focal point shifting in the coronal plane by a max of 2 mm from the targeted focal point and away from transducer ($p < 0.01$) (Figure 5-7 and Figure 5-8). Since a similar focal shift was noticed in both full skull and half skull specimen, we conclude that the reverberation due to the base of the skull isn't a concern, at this time, based on the parameters and the target chosen.

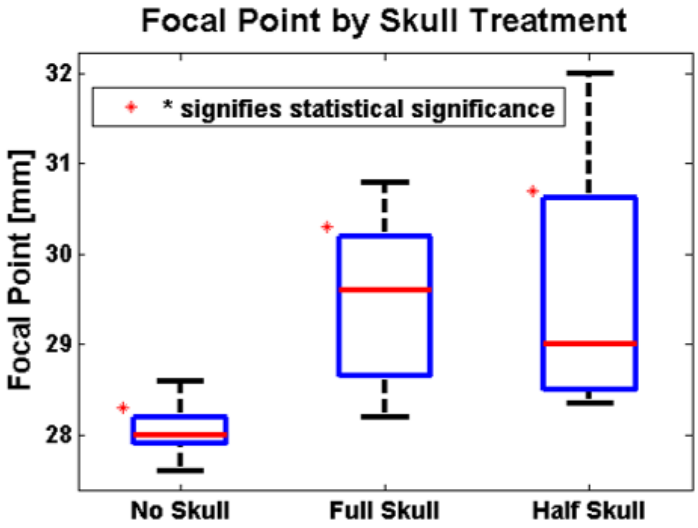

Figure 5-7 : Box plots of focal points/position

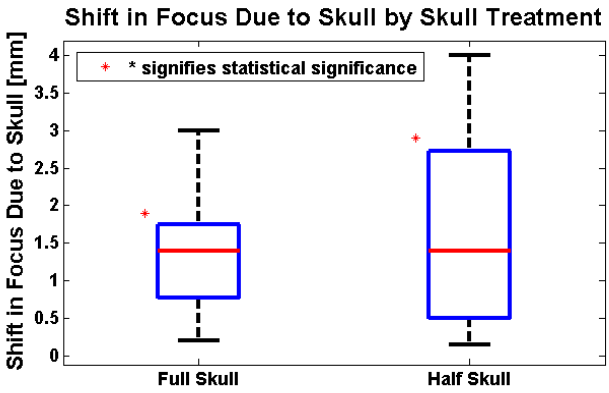

Figure 5-8 : Box plots of focal shift due to full/half skull compared to no skull

Repeated focal measurement of the same specimen, both full and half skull, revealed that the shifts are highly reproducible per specimen. The maximum focal shift variation when measuring the same full skull and half skull are 0.2 mm and 0.5 mm, respectively (Figure 5-8). This indicates that the standard deviation in the data set is not due to the measurement apparatus but rather due to the natural variation in the skull morphology, which causes each skull to have a unique effect. This minor variation in repeating focal shift per specimen was achieved as a result of careful set up procedures which highlights the significance of skull configuration and the orientation relative to the transducer. The correct alignment of the skull with respect to the transducer is very crucial and should be given a lot of attention during *in vivo* studies to avoid target variation from one specimen to another especially in small animal models.

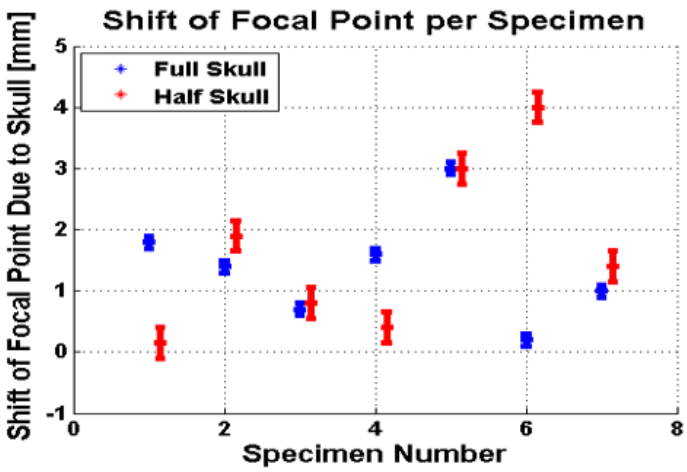

Figure 5-9 : Focal shit of all specimens. Error bars represent work of intra-observer repeatability study

Raster scans conducted at the focal plane revealed that there is 0.5mm to 1 mm shift in the transverse plane due to the top half of the skull (Figure 5-10). The raster scan results from three of the skull specimen are presented in Figure 5-10. Figure 5-10a illustrates the planar contour of the acoustic beam at the focal plane with no skull specimen present. Figure 5-10b illustrates the deformation of the ultrasound acoustic beam and the focal shift of 0.5 mm to 1 mm with a half skull . The transverse shift also was highly dependent on the orientation of the skull relative to the transducer during the experiment set up.

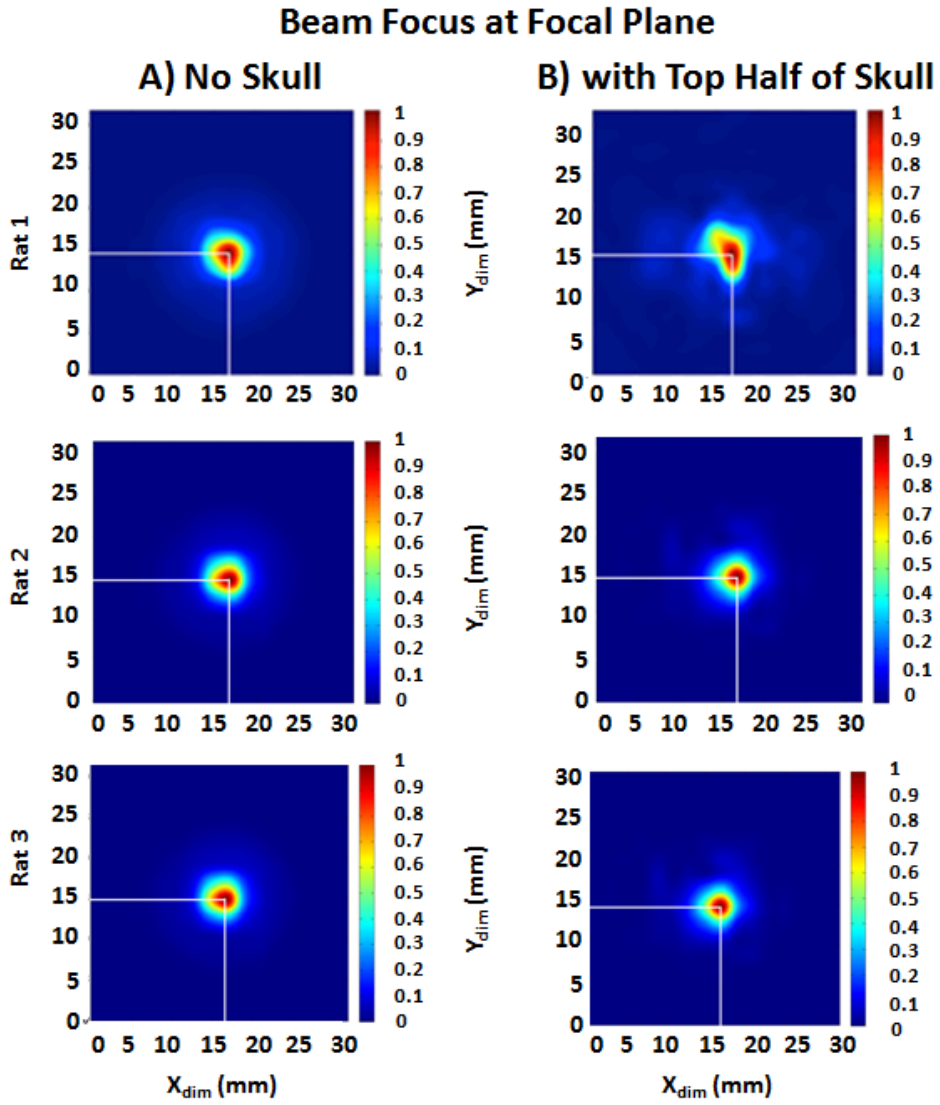

Figure 5-10 : Beam targeting and deflection studies through raster scanning focal planes of no skull (A) and top half of skull specimens (B)

In summary, the degree of the focal shift is specific to each skull, with excellent reproducibility, implying that skull-specific compensation for beam deformation may be necessary for clinical translation . We did not encounter major concerns due to reverberation since we used low duty cycle and intensity. However further studies should explore longer duty cycles, and multiple targets inside the skull. In addition, across all 9 skulls, our results revealed substantial ultrasonic intensity attenuation on the order of 40% ± 4% (Figure 5-11).

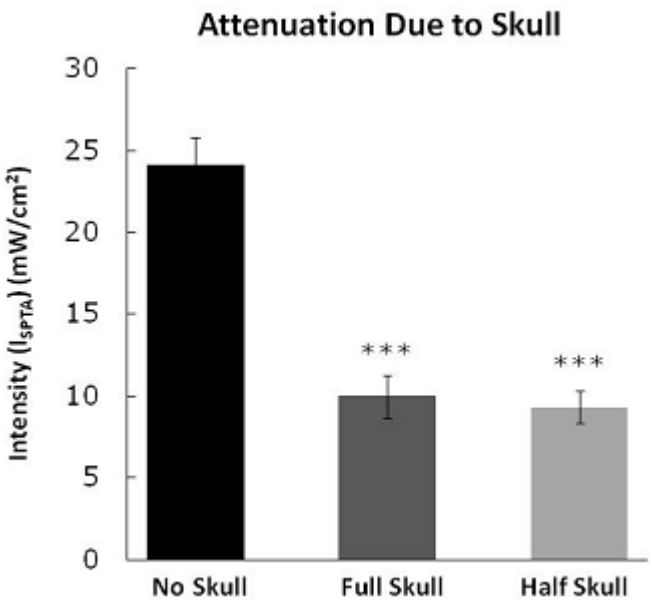

Figure 5-11: Full and half skull effect on intensity attenuation

Attenuation and acoustic targeting has not been considered a major concern in murine models due to the small size of the rat brain, and thin top skull layer especially for non-focused ultrasound experiments. However, the acoustic focal dimensions of a focused ultrasound that we investigated were 3 mm in diameter and 1.5 mm in height, which experienced a focal shift due to the skull. Therefore, the focus missed the target in the coronal direction which was 1 mm in our studies. We conclude that a minimum of 3-4 mm target height was necessary for correct targeting in our studies. In addition, if the target is close to the base of the skull, then the shift could result in reflections which can cause secondary focal points away from the original focus within the brain. Therefore precise acoustic characterization inside skull models will improve our ability to compensate for the effects of the skull and improve targeting for future *in vivo* studies.

Conclusion

A possible contributor to low success rate in non-invasive transcranial ultrasound neuromodulation is the common disregard for the effect of the skull on ultrasonic beam shape

and targeting of neural structures in rat models. Our studies have shown that during transcranial sonication of the rat skull the LIFU beam shape is deformed. In addition, transcranial sonication results in substantial attenuation of LIFU intensity combined with significant shifting of the focus in both the coronal and transverse planes of up to 2mm. Thus further experiments exploring different frequencies and multiple targets, simulations, and expanding studies to larger animal models such as pigs and human will improve the understanding of the barriers presented by transcranial passage for targeting accuracy in *in vivo* applications.

5.4 Conclusion

A possible contributor to low success rate in non-invasive transcranial ultrasound neuromodulation is the common disregard for the effect of the skull on ultrasonic beam shape and targeting of neural structures in rat models. Our studies have shown that during transcranial sonication of the rat skull the LIFU beam shape is deformed. In addition, transcranial sonication results in substantial attenuation of LIFU intensity combined with significant shifting of the focus in both the coronal and transverse planes of up to 2mm. Thus further experiments exploring different frequencies and multiple targets, simulations, and further expanding studies to larger animal models such as pigs and human will improve the understanding of the barriers presented by transcranial passage for targeting accuracy in *in vivo* applications.

6 Conclusions and Future Directions

Recent *in vivo* studies have revealed promising neuromodulation results using low intensity focused ultrasound (LIFU) suggesting that LIFU may be a non-invasive alternative therapy for neurological disease such as Parkinson's and epilepsy [26, 48]. Despite these recent successful results, there is a low rate of repeatability and we believe that this is, in part, due to a knowledge gap around the mechanism of LIFU stimulation, the lack of data exploring the large LIFU parameter, and the impact of the skull on targeting accuracy in *in vivo* transcranial sonication. The challenges of mechanism and targeting were addressed in this thesis to enable more reliable future *in vivo* results with improved precision.

While mechanism underlying lower-intensity neuromodulation stays unknown, it has been suggested that ultrasound exposure induces mechanical perturbation on cellular membrane which results in stimulation of the embedded protein channel kinetics leading to depolarization, and ultimately, to increased neural activity. Debate continues on whether the acoustic pressure transmission is generated due to the formation and collapse of gaseous cavitation bubbles adjacent to cellular membrane [81], or due to a non-cavitation mechanisms resulting from acoustic radiation propagating through the medium, modulating cellular membrane channels [12]. Regardless, both sources of pressure are thought to modulate ion-channel kinetics.

In order to enable LIFU mechanism studies, a novel low frequency ultrasonic array transducer and a single element focused transducer system with different frequencies were developed and characterized. Both systems were designed to be compatible with well plates for *in vitro* studies.

Despite the conventional hypothesis, our recent experiments using simplified liposome and proteoliposome models tested the mechanosensitive (MscL) and non mechanosensitive (Na2K

and KVAP) channel activity as a result of ultrasound sonication. The model was specifically designed to focus on protein and liposome interaction and did not take cellular cytoskeleton and other structures into account. The results revealed an increase in efflux through proteoliposomes regardless of the channel type except at the highest concentration of mechanosensitive channel (MS) model where a lower efflux was noticed. These unexpected results suggest that focused ultrasound does not modulate the gating of ion channels, using 500 kHz frequency and our parameter set and system design, but instead affects the permeability of the membrane itself or protein-membrane interface. Also a dual effect of membrane stretch enhancement and pore formation is observed only at high MS channel concentration. The MscL channel at a certain concentration is able to relief the pressure imposed on the membrane by stretching and acting as a damper that reduces leakage through membrane or protein-membrane interface. Other statistical models will be considered in future work to improve the statistical significance and data analysis.

To prepare for *in vivo* efficacy studies, the present dissertation characterized the ultrasonic beam scatter and focal shifts that occur as ultrasound passes through a rat skull for a specific set of parameters. The results revealed that during transcranial sonication of the rat skull the LIFU beam shape was deformed substantially, likely leading to a shift in the target. In addition, transcranial sonication results in substantial attenuation of LIFU intensity combined with significant shifting of the focus in the coronal plane of up to 2mm. The skull effect on the beam can be further explored by varying frequency and different target points. In addition, simulations of the conducted studies

Therefore, our results suggest a new understanding of mechanisms explaining lower-intensity ultrasound modulation while also improving targeting abilities with better accuracy and precision for future *in vivo* studies.

The reported *in vitro* studies can be extended to more realist cell models that include cytoskeleton to explore the effect of cytoskeleton on protein-lipid interaction during sonication. Different frequencies, parameter sets and system designs should be explored. In addition, targeting studies should be extended to multiple frequencies and target points inside the skull. Also our *ex vivo* experiment should be repeated using a simulation model to verify the focal shift findings and expand the simulation model to larger animal and human skull.

These suite of studies will hopefully allow us to optimize our focused ultrasound beam and the associated parameters to achieve a higher success rate of neuromodulation in future pre-clinical, and ultimately clinical, models.

7 References

1. Engel, J., et al., *Practice parameter: Temporal lobe and localized neocortical resections for epilepsy Report of the Quality Standards Subcommittee of the American Academy of Neurology, in Association with the American Epilepsy Society and the American Association of Neurological Surgeons.* Neurology, 2003. **60**(4): p. 538-547.
2. Cantello, R., et al., *Slow Repetitive TMS for Drug-resistant Epilepsy: Clinical and EEG Findings of a Placebo-controlled Trial.* Epilepsia, 2007. **48**(2): p. 366-374.
3. Joo, E.Y., et al., *Antiepileptic effects of low-frequency repetitive transcranial magnetic stimulation by different stimulation durations and locations.* Clinical neurophysiology, 2007. **118**(3): p. 702-708.
4. Fregni, F., et al., *A randomized clinical trial of repetitive transcranial magnetic stimulation in patients with refractory epilepsy.* Annals of neurology, 2006. **60**(4): p. 447-455.
5. Chkhenkeli, S.A., et al., *Electrophysiological effects and clinical results of direct brain stimulation for intractable epilepsy.* Clinical neurology and neurosurgery, 2004. **106**(4): p. 318-329.
6. DeGiorgio, C.M., et al., *Randomized controlled trial of trigeminal nerve stimulation for drug-resistant epilepsy.* Neurology, 2013. **80**(9): p. 786-791.
7. Rossi, S., et al., *Safety, ethical considerations, and application guidelines for the use of transcranial magnetic stimulation in clinical practice and research.* Clinical neurophysiology, 2009. **120**(12): p. 2008-2039.
8. King, R.L., et al., *Effective parameters for ultrasound-induced in vivo neurostimulation.* Ultrasound in medicine & biology, 2013. **39**(2): p. 312-331.
9. Tyler, W.J., *Noninvasive neuromodulation with ultrasound? A continuum mechanics hypothesis.* The Neuroscientist, 2011. **17**(1): p. 25-36.
10. Min, B.-K., et al., *Focused ultrasound-mediated suppression of chemically-induced acute epileptic EEG activity.* BMC neuroscience, 2011. **12**(1): p. 23.
11. Tufail, Y., et al., *Transcranial pulsed ultrasound stimulates intact brain circuits.* Neuron, 2010. **66**(5): p. 681-694.
12. Tyler, W.J., et al., *Remote excitation of neuronal circuits using low-intensity, low-frequency ultrasound.* PLoS One, 2008. **3**(10): p. e3511.
13. Johns, L.D., *Nonthermal effects of therapeutic ultrasound: the frequency resonance hypothesis.* Journal of athletic training, 2002. **37**(3): p. 293.
14. Wood, R.W. and A.L. Loomis, *XXXVIII. The physical and biological effects of high-frequency sound-waves of great intensity.* The London, Edinburgh, and Dublin Philosophical Magazine and Journal of Science, 1927. **4**(22): p. 417-436.
15. Martinez, D., *Therapeutic Ultrasound: A Review of the Literature*. 2010, Chiro Access.

16. Clement, G., J. White, and K. Hynynen, *Investigation of a large-area phased array for focused ultrasound surgery through the skull.* Physics in medicine and biology, 2000. **45**(4): p. 1071.

17. McDannold, N., et al., *Transcranial MRI-guided focused ultrasound surgery of brain tumors: Initial findings in three patients.* Neurosurgery, 2010. **66**(2): p. 323.

18. Bailey, M., et al., *Physical mechanisms of the therapeutic effect of ultrasound (a review).* Acoustical Physics, 2003. **49**(4): p. 369-388.

19. Dewhirst, M., et al., *Basic principles of thermal dosimetry and thermal thresholds for tissue damage from hyperthermia.* International Journal of Hyperthermia, 2003. **19**(3): p. 267-294.

20. Sapareto, S.A. and W.C. Dewey, *Thermal dose determination in cancer therapy.* International Journal of Radiation Oncology* Biology* Physics, 1984. **10**(6): p. 787-800.

21. ter Haar, G., *Therapeutic applications of ultrasound.* Progress in biophysics and molecular biology, 2007. **93**(1): p. 111-129.

22. Hynynen, K. and G. Clement, *Clinical applications of focused ultrasound-the brain.* International Journal of Hyperthermia, 2007. **23**(2): p. 193-202.

23. Fry, W. and F. Fry, *Fundamental Neurological Research and Human Neurosurgery Using Intense Ultrasound.* Phys. Med, 1958. **37**: p. 148.

24. Adrianov, O., N. Vykhodtseva, and L. Gavrilov, *[Use of focused ultrasound for local effects on deep brain structures].* Fiziologicheskii zhurnal SSSR imeni IM Sechenova, 1984. **70**(8): p. 1157-1166.

25. Gavrilov, L., et al., *The effect of focused ultrasound on the skin and deep nerve structures of man and animal.* Progress in brain research, 1976. **43**: p. 279-292.

26. Gavrilov, L.R., E.M. Tsirul'nikov, and E.E. Shchekanov, *[Responses of the auditory centers of the frog midbrain to labyrinth stimulation by focused ultrasound].* Fiziol Zh SSSR Im I M Sechenova, 1975. **61**(2): p. 213-21.

27. Fry, W., et al., *Physical Factors Involved in Ultrasonically Induced Changes in Living Systems: I. Identification of Non-Temperature Effects.* The Journal of the Acoustical Society of America, 1950. **22**(6): p. 867-876.

28. Foley, J.L., et al., *Image-guided HIFU neurolysis of peripheral nerves to treat spasticity and pain.* Ultrasound in medicine & biology, 2004. **30**(9): p. 1199-1207.

29. Lynn, J.G. and T.J. Putnam, *Histology of cerebral lesions produced by focused ultrasound.* The American journal of pathology, 1944. **20**(3): p. 637.

30. Lynn, J.G., et al., *A new method for the generation and use of focused ultrasound in experimental biology.* The Journal of general physiology, 1942. **26**(2): p. 179.

31. Fry, W.J., *Intense ultrasound in investigations of the central nervous system.* Adv Biol Med Phys, 1958. **6**: p. 281-348.

32. Jagannathan, J., et al., *High intensity focused ultrasound surgery (HIFU) of the brain: A historical perspective, with modern applications.* Neurosurgery, 2009. **64**(2): p. 201.

33. Lipsman, N., et al., *MR-guided focused ultrasound thalamotomy for essential tremor: a proof-of-concept study.* The Lancet Neurology, 2013. **12**(5): p. 462-468.

34. Elias, W.J., et al., *A pilot study of focused ultrasound thalamotomy for essential tremor.* New England Journal of Medicine, 2013. **369**(7): p. 640-648.

35. Ballantine Jr, H., E. Bell, and J. Manlapaz, *Progress and problems in the neurological applications of focused ultrasound.* Journal of neurosurgery, 1960. **17**: p. 858-876.

36. Young, R.R. and E. Henneman, *Functional effects of focused ultrasound on mammalian nerves.* Science, 1961. **134**(3489): p. 1521-1522.

37. Vykhodtseva, N.I., et al., *[Use of focused ultrasound for local destruction of different brain structures].* Zh Nevropatol Psikhiatr Im S S Korsakova, 1976. **76**(12): p. 1810-6.

38. Gavrilov, L.R., et al., *A study of reception with the use of focused ultrasound. I. Effects on the skin and deep receptor structures in man.* Brain research, 1977. **135**(2): p. 265-277.

39. Vykhodtseva, N., K. Hynynen, and C. Damianou, *Histologic effects of high intensity pulsed ultrasound exposure with subharmonic emission in rabbit brain in vivo.* Ultrasound in medicine & biology, 1995. **21**(7): p. 969-979.

40. Vykhodtseva, N., et al., *[Characteristics of the formation of local destructive foci in brain tissues exposed to focused ultrasound].* Biulleten'eksperimental'noi biologii i meditsiny, 1985. **99**(6): p. 689-693.

41. Mihran, R.T., F.S. Barnes, and H. Wachtel, *Transient modification of nerve excitability in vitro by single ultrasound pulses.* Biomed Sci Instrum, 1990. **26**: p. 235-46.

42. Warden, S., et al., *Acceleration of fresh fracture repair using the sonic accelerated fracture healing system (SAFHS): a review.* Calcified Tissue International, 2000. **66**(2): p. 157-163.

43. Tsui, P.-H., S.-H. Wang, and C.-C. Huang, *In vitro effects of ultrasound with different energies on the conduction properties of neural tissue.* Ultrasonics, 2005. **43**(7): p. 560-565.

44. Dalecki, D., *Mechanical bioeffects of ultrasound.* Annu. Rev. Biomed. Eng., 2004. **6**: p. 229-248.

45. O'Brien, W.D., *Ultrasound–biophysics mechanisms.* Progress in biophysics and molecular biology, 2007. **93**(1): p. 212-255.

46. Tufail, Y., et al., *Ultrasonic neuromodulation by brain stimulation with transcranial ultrasound.* nature protocols, 2011. **6**(9): p. 1453-1470.

47. Yoo, S.-S., et al., *Focused ultrasound modulates region-specific brain activity.* Neuroimage, 2011. **56**(3): p. 1267-1275.

48. Kim, H., et al., *Noninvasive transcranial stimulation of rat abducens nerve by focused ultrasound.* Ultrasound in medicine & biology, 2012. **38**(9): p. 1568-1575.

49. Krasovitski, B., et al., *Intramembrane cavitation as a unifying mechanism for ultrasound-induced bioeffects.* Proceedings of the National Academy of Sciences, 2011. **108**(8): p. 3258-3263.

50. Nyborg, W., *Ultrasonic microstreaming and related phenomena.* The British journal of cancer. Supplement, 1982. **5**: p. 156.

51. Menon, G.K., D. Bommannan, and P. Elias, *High-frequency sonophoresis: permeation pathways and structural basis for enhanced permeability.* Skin Pharmacology and Physiology, 1994. **7**(3): p. 130-139.

52. Tachibana, K., et al., *Enhanced cytotoxic effect of Ara-C by low intensity ultrasound to HL-60 cells.* Cancer letters, 2000. **149**(1): p. 189-194.

53. Pong, M., et al., *In vitro ultrasound-mediated leakage from phospholipid vesicles.* Ultrasonics, 2006. **45**(1): p. 133-145.

54. Kagiya, G., et al., *Expression of heme oxygenase-1 due to intracellular reactive oxygen species induced by ultrasound.* Ultrasonics sonochemistry, 2006. **13**(5): p. 388-396.

55. Sato, W., T. Matsushita, and K. Nakamura, *Acceleration of increase in bone mineral content by low-intensity ultrasound energy in leg lengthening.* Journal of ultrasound in medicine, 1999. **18**(10): p. 699-702.

56. Carmen, J., et al., *Ultrasonically enhanced vancomycin activity against Staphylococcus epidermidis biofilms in vivo.* Journal of biomaterials applications, 2004. **18**(4): p. 237-245.

57. Pitt, W.G., et al., *Ultrasonic enhancement of antibiotic action on gram-negative bacteria.* Antimicrobial agents and chemotherapy, 1994. **38**(11): p. 2577-2582.

58. Leighton, T., *The acoustic bubble*. 2012: Academic press.

59. Babakhanian, M., et al. *In vitro cell system for studying molecular mechanisms of action associated with low intensity focused ultrasound*. in *SPIE BiOS*. 2012. International Society for Optics and Photonics.

60. Gaitatzis, A. and J.W. Sander, *The long-term safety of antiepileptic drugs.* CNS drugs, 2013. **27**(6): p. 435-455.

61. Vonck, K., et al., *Neurostimulation for refractory epilepsy.* Acta neurologica belgica, 2003. **103**(4): p. 212-217.

62. Fitzgerald, P.B. and Z.J. Daskalakis, *The effects of repetitive transcranial magnetic stimulation in the treatment of depression.* 2011.

63. Harvey, E.N., *The effect of high frequency sound waves on heart muscle and other irritable tissues.* American Journal of Physiology--Legacy Content, 1929. **91**(1): p. 284-290.

64. Wulff, V., et al., *Effects of Ultrasonic Vibrations on Nerve Tissues.* Experimental Biology and Medicine, 1951. **76**(2): p. 361-366.

65. Deffieux, T., et al., *Low-intensity focused ultrasound modulates monkey visuomotor behavior.* Current Biology, 2013. **23**(23): p. 2430-2433.

66. Glaasker, E., et al., *Mechanism of osmotic activation of the quaternary ammonium compound transporter (QacT) of Lactobacillus plantarum.* Journal of bacteriology, 1998. **180**(21): p. 5540-5546.

67. van der Heide, T. and B. Poolman, *Osmoregulated ABC-transport system of Lactococcus lactis senses water stress via changes in the physical state of the membrane.* Proceedings of the National Academy of Sciences, 2000. **97**(13): p. 7102-7106.

68. Moe, P. and P. Blount, *Assessment of potential stimuli for mechano-dependent gating of MscL: effects of pressure, tension, and lipid headgroups.* Biochemistry, 2005. **44**(36): p. 12239-12244.

69. Sukharev, S.I., et al., *A large-conductance mechanosensitive channel in E. coli encoded by mscL alone.* Nature, 1994. **368**(6468): p. 265-268.

70. Boucher, P.-A., C.E. Morris, and B. Joos, *Mechanosensitive closed-closed transitions in large membrane proteins: osmoprotection and tension damping.* Biophysical journal, 2009. **97**(10): p. 2761-2770.

71. Moe, P.C., P. Blount, and C. Kung, *Functional and structural conservation in the mechanosensitive channel MscL implicates elements crucial for mechanosensation.* Molecular microbiology, 1998. **28**(3): p. 583-592.

72. Levina, N., et al., *Protection of Escherichia coli cells against extreme turgor by activation of MscS and MscL mechanosensitive channels: identification of genes required for MscS activity.* The EMBO Journal, 1999. **18**(7): p. 1730-1737.

73. Powl, A.M., J.M. East, and A.G. Lee, *Anionic Phospholipids Affect the Rate and Extent of Flux through the Mechanosensitive Channel of Large Conductance MscL†.* Biochemistry, 2008. **47**(14): p. 4317-4328.

74. Yang, L.-M., et al., *Three routes to modulate the pore size of the MscL channel/nanovalve.* ACS nano, 2012. **6**(2): p. 1134-1141.

75. Iscla, I., et al., *Improving the design of a MscL-based triggered nanovalve.* Biosensors, 2013. **3**(1): p. 171-184.

76. Perozo, E., et al., *Physical principles underlying the transduction of bilayer deformation forces during mechanosensitive channel gating.* Nature Structural & Molecular Biology, 2002. **9**(9): p. 696-703.

77. Sukharev, S., S.R. Durell, and H.R. Guy, *Structural models of the MscL gating mechanism.* Biophysical journal, 2001. **81**(2): p. 917-936.

78. Azuma, T., et al. *Schlieren observation of therapeutic field in water surrounded by cranium radiated from 500 kHz ultrasonic sector transducer*. in *Ultrasonics Symposium, 2004 IEEE*. 2004. IEEE.

79. O'Reilly, M.A., Y. Huang, and K. Hynynen, *The impact of standing wave effects on transcranial focused ultrasound disruption of the blood–brain barrier in a rat model.* Physics in medicine and biology, 2010. **55**(18): p. 5251.

80. Younan, Y., et al., *Influence of the pressure field distribution in transcranial ultrasonic neurostimulation.* Medical physics, 2013. **40**(8): p. 082902.

81. Juffermans, L.J., et al., *Low-intensity ultrasound-exposed microbubbles provoke local hyperpolarization of the cell membrane via activation of BK Ca channels.* Ultrasound in medicine & biology, 2008. **34**(3): p. 502-508.